

## NEAR-INFRARED VARIABILITY OF LOW MASS STARS IN IC 1396A AND TR 37

HUAN Y. A. MENG<sup>1</sup>, G. H. RIEKE<sup>1</sup>, JINYOUNG SERENA KIM<sup>1</sup>, AURORA SICILIA-AGUILAR<sup>2</sup>, N. J. G. CROSS<sup>3</sup>, TARAN ESPLIN<sup>1</sup>, L. M. REBULL<sup>4</sup>, KLAUS W. HODAPP<sup>5</sup>

*Draft v8.0*

### ABSTRACT

We have monitored nearly a square degree in IC 1396A/Tr 37 over 21 epochs extending over 2014 – 2016 for sources variable in the *JHK* bands. In our data,  $65 \pm 8$  % of previously identified cluster members show variations, compared with  $\lesssim 0.3\%$  of field stars. We identify 119 members of Tr 37 on the basis of variability, forming an unbiased sample down to the brown dwarf regime. The *K*-band luminosity function in Tr 37 is similar to that of IC 348 but shifted to somewhat brighter values, implying that the *K*- and *M*-type members of Tr 37 are younger than those in IC 348. We introduce methods to classify the causes of variability, based on behavior in the color-color and color-magnitude diagrams. Accretion hot spots cause larger variations at *J* than at *K* with substantial scatter in the diagrams; there are at least a dozen, with the most active resembling EXors. Eleven sources are probably dominated by intervention of dust clumps in their circumstellar disks with color behavior indicating the presence of grains larger than for interstellar dust, presumably due to grain growth in their disks. Thirteen sources have larger variations at *K* than at *J* or *H*. For 11 of them, the temperature fitted to the variable component is very close to 2000K, suggesting that the changes in output are caused by turbulence at the inner rim of the circumstellar disk exposing previously protected populations of grains.

*Keywords:* protoplanetary disks — infrared: planetary systems — infrared: stars — stars: pre-main sequence — open clusters and associations: individual (Tr 37)

### 1. INTRODUCTION

Variability is a very common characteristic of young stellar objects (YSOs) and young sub-stellar objects (YSOs). However, its prevalence only became apparent with systematic surveys conducted with, for example, the 2-Micron All Sky Survey (2MASS) (Skrutskie et al. 2006) and with *Spitzer* (Werner et al. 2004). The underlying causes for this behavior are only partially understood, but can include variable accretion rates, magnetic activity, flares, hot or cold starspots, and the effects of circumstellar disks such as changes in extinction or disk emission. A better understanding of the variation patterns can therefore give insight to many aspects of YSO behavior, including fundamental ones such as accretion and the structure of protoplanetary disks.

Optical and infrared (IR) variability studies have also been used as a powerful tool to identify candidate YSOs. At faint limits the colors of reddened background stars can mimic faint cluster members. This issue can be combated with multiple observations to identify members by variability, since only a tiny fraction of field stars are variable (e.g., Morales-Calderón et al. 2009; Pietrukowicz et al. 2009; Wolk et al. 2013a,b).

To use variability as a tool to probe YSOs requires systematic surveys extending over long time baselines. For example, the YSOVAR program in the warm *Spitzer* mission (PI J. Stauffer) monitored selected regions intensively for about a month twice a year (due to visibility constraints) (Rebull et al. 2014). In the Orion nebula cluster (ONC) this effort found that 77% of disked stars and 44% of the weak-lined T Tauri Stars (WTTS) showed variations (Morales-Calderón et al. 2011). Rice et al. (2015) used the Wide Field Camera (WFCAM) on the United Kingdom Infrared Telescope (UKIRT) to carry out a very extensive *JHK* study of the same region, finding 1203 variable stars. Rice et al. (2012); Wolk et al. (2013a,b) also used WFCAM to monitor Cyg OB7 over 1.5 years showing that 83% of known YSOs are variable and less than 2% of the field stars are. They found about 60 short period (a few days) variables, a similar number of stochastic variables, a number of stars with long periods (20 - 60 days), and about 25 with unclassified variations. Other examples of near-infrared variability surveys include Orion A by Carpenter et al. (2001) using 2MASS data and  $\rho$  Oph by de Oliveira & Casali (2008) with UKIRT/WFCAM.

The number of such studies is modest, but they have proven to give unique insights in areas like young star gas accretion and the structure of protoplanetary disks. To complement them, we have carried out a multi-epoch deep near-IR imaging variability survey of the star forming region IC 1396A/Tr 37 using UKIRT/WFCAM. Our target region covers a range of ages from  $< 0.5$  Myr to 10 Myr, and we have monitored this region with 21 epochs of observation extending over nearly two years. We are able to obtain accurate variability and color information down to  $K \sim 17$  mag, allowing a deep search for very

Electronic address: hyameng@lpl.arizona.edu

<sup>1</sup> Steward Observatory, Department of Astronomy, University of Arizona, 933 North Cherry Avenue, Tucson, AZ 85721

<sup>2</sup> SUPA, School of Science and Engineering, University of Dundee, Nethergate, Dundee DD1 4HN, UK

<sup>3</sup> Wide-Field Astronomy Unit, Institute for Astronomy, School of Physics and Astronomy, University of Edinburgh, Royal Observatory, Blackford Hill, Edinburgh EH9 3HJ, UK

<sup>4</sup> Spitzer Science Center, Infrared Processing and Analysis Center, California Institute of Technology, 1200 E. California Blvd., Pasadena, CA 91125

<sup>5</sup> Institute for Astronomy, University of Hawaii, 640 N. Aohoku Place, Hilo, HI 96720, USA

low mass cluster members down into the brown dwarf regime.

IC 1396A is a bright-rimmed globule complex, also known as “the Elephant Trunk Nebula”, illuminated by HD 206267, a Trapezium-like O star system (O6.5V + O9V), which is a part of Cepheus OB2 association, and is at a distance of  $945_{-73}^{+90}$  pc from Gaia DR2 measurements (Gaia Collaboration 2018; Sicilia-Aguilar et al. 2019). This value is consistent within the errors with the result from main sequence fitting of the intermediate mass ( $\sim$  A-type) stars,  $870 \pm 80$  pc (Contreras et al. 2002), particularly given a possible small bias in the Gaia results toward large distances (Xu et al. 2019). IC 1396A is at the western edge of the Tr 37 cluster (Marschall & van Altena 1987; Platais et al. 1998). Sicilia-Aguilar et al. (2004, 2005, 2006a, 2013) have conducted observations of Tr 37 using optical photometric and spectroscopic data as well as *Spitzer* IRAC and MIPS in the IR to identify and study the young stellar population and circumstellar disk evolution. YSOs in Tr 37 have also been studied in the X-ray using the *Chandra* X-ray Observatory (Getman et al. 2012) and far-IR using the *Herschel* Space Observatory (Sicilia-Aguilar et al. 2015). From these studies, the Cep OB2 association harbors multiple generations of star forming regions (Sicilia-Aguilar et al. 2005, 2006b, 2019; Morales-Calderón et al. 2009): NGC 7160 (10-12 Myr), Tr 37 (3-4 Myr), IC 1396A and IC 1396N ( $\lesssim 1$  Myr). It provides an ideal laboratory to study YSO disk evolution under an external UV radiation environment in multiple evolutionary phases, since the typical lifetimes of gaseous disks around low mass stars are  $\lesssim 3 - 5$  Myr (e.g., Ribas et al. 2015; Meng et al. 2017).

Sicilia-Aguilar et al. (2005) presented a list of optically variable sources in this region based on about a week of monitoring, and Barentsen et al. (2011) presented  $r$  and  $i$  variable sources from “several” nights of their IPHAS survey, which covered a  $7 \text{ deg}^2$  region in Cep OB2 that included IC 1396. Mid-IR variability in the IC 1396A region has been studied with *Spitzer* by Morales-Calderón et al. (2009). This study conducted two modes of observations: a 14 day time span with twice a day cadence as well as 7 hours of continuous “staring” mode observations, and found that more than 50% of the YSOs were variable. Scholz et al. (2010) monitored IC 1369W with WFCAM in JHK intensively for three nights, discovering two eclipsing binaries and eight periodic variables.

We have built on this previous work by conducting a long-term (2 year span) variability study of Tr 37 ( $53' \times 53'$  field of view) in the near-IR ( $J, H, K$ ) using UKIRT/WFCAM (Figure 1). This study includes the globule IC 1396A and an additional nearby area (the north-western region from IC 1396A) to probe a less-studied part of Tr 37. In Section 2, we describe our observations and the data reduction. In Section 3 we present the results and our analysis of variability, including variable source selection criteria. In Section 4 we compare our results with previous variability studies, then discuss (1) the variability of bright members in Tr 37, (2) variable low mass members, (3) new variable member candidates using a color-magnitude diagram analysis to test whether variable stars are likely to be cluster members, and (4) characteristics of the highly varying sources. We show that although it has been thought that Tr 37 and

IC 348 YSOs are similar in age, the  $K$ -band luminosity function and  $K$  vs.  $I - K$  isochrone of Tr 37 are shifted brighter by  $\sim 0.3 - 0.5$  mag, indicating that the stars in Tr 37 are younger than those in IC 348. We then introduce simple methods to distinguish different causes of variations: (1) accretion hot spots cause larger changes at  $J$  than at  $K$ , and significant scatter in colors, both of which can be identified in appropriate color-color and color-magnitude diagrams; (2) extinction variations have a distinctive track on such diagrams, with little scatter around it; and (3) sources with larger variations at  $K$  due to sporadic illumination of disk dust tend to fall on or below the CTTS locus on  $J - H$ ,  $H - K$  diagrams. We conclude that: (a) the wavelength dependence of the extinction from the circumstellar disks is noticeably affected by grain growth in the disks; (b) four sources show extreme variability and may be related to EXors; (c) the sources that vary predominantly at  $K$  nearly all show a color temperature near 2000K for the variable component, suggesting the variations arise from dust exposed by turbulence at the inner edge of the circumstellar disk; and (d) at least one source appears to have been obscured for an extended period by an optically thick disk component. A summary and our conclusions follow in section 5.

## 2. OBSERVATIONS AND DATA REDUCTION

### 2.1. Observations

Observations were conducted in  $J, H, K$  bands with the Wide Field Camera (WFCAM) (Casali et al. 2007) on the United Kingdom Infrared Telescope (UKIRT) on Mauna Kea, Hawaii. The focal plane hosts four Rockwell Hawaii-II HgCdTe detectors laid out in a  $2 \times 2$  array. Each detector has  $2048 \times 2048$  pixels with a pixel scale of  $0.4'' \text{ pixel}^{-1}$ , covering  $13.65'$  on one side. Adjacent detector arrays are separated by a gap  $12.8'$  in width. To fill the gaps and maximize the sky coverage, we dithered the telescope at four positions with a  $13.2' \times 13.2'$  square pattern, so the detector gaps in one exposure were covered in the previous/next exposure with narrow strips of overlap, yielding the image displayed in Figure 1. The total sky coverage was a  $53' \times 53'$  square, ranging from  $323.082^\circ$  to  $324.752^\circ$  in RA and from  $57.196^\circ$  to  $58.080^\circ$  in Dec. The integration time of each exposure was 10 s, 5 s, and 5 s in  $J$ ,  $H$ , and  $K$ , respectively. Each run consisted of 20 consecutive exposures in each waveband, i.e., total integrations of 200, 100, and 100 s respectively. The instrumentation and observing strategy were similar to those used in a number of previous studies of young star variability (e.g., Rice et al. 2012; Wolk et al. 2013b; Rice et al. 2015).

The same observational design was executed in all three bands at each epoch on the same field to ensure data homogeneity across time. From July 18, 2014, to July 12, 2016, we have 21 epochs in total<sup>6</sup> over a time baseline of 725 days, or almost 2 years. The observation start time of each epoch is given in Table 1. Some epochs have more than one run in some bands, as indicated in the notes in Table 1. The seeing ranged from  $0.6''$  at best to  $1.4''$  at worst, with an average of  $0.79''$ . Although our cadence does not allow study of periodicity, the number

<sup>6</sup> Not including incomplete observations due to bad weather conditions.

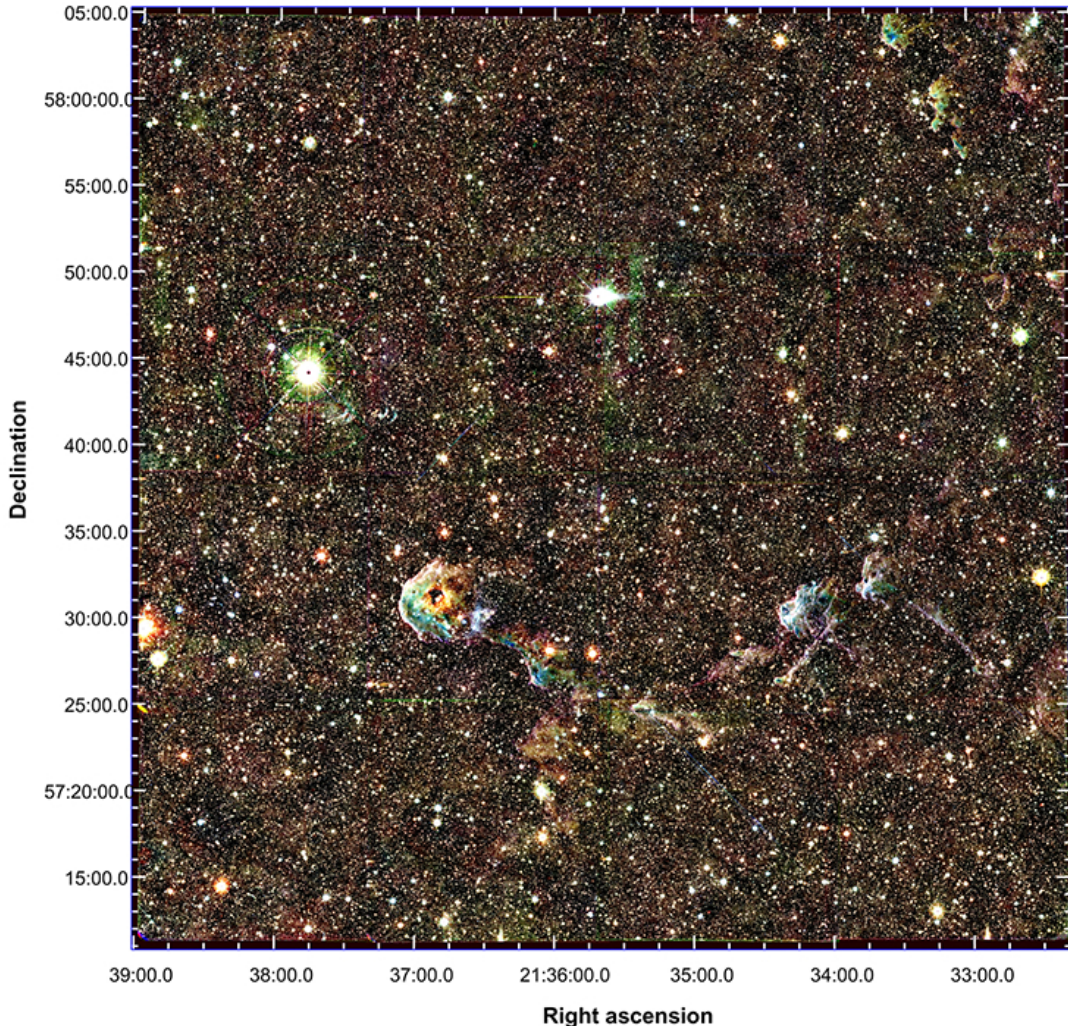


**Figure 1.** A color composite image of TR 37 using UKIRT/WFCAM (blue:  $J$ , green:  $H$ , red:  $K$ ). North is up and east is to the left. The coverage was chosen to avoid the bright O6.5+O9 star system HD 206267 (which is located just off the field of view toward the left illuminating the IC 1396A globule) and to focus on the less studied region to the northwest of the nebula head.

of epochs is sufficient to identify the great majority of variable stars (Rice et al. 2012, 2015).

## 2.2. Data Reduction

The science images were prepared by the UKIRT/WFCAM pipeline at the Cambridge Astronomical Survey Unit (CASU) (Irwin et al. 2004; Hodgkin et al. 2009). They were stored in the WFCAM Science Archive<sup>7</sup> (Hambly et al. 2008), where they were also checked for quality and organized for various retrieval strategies. The pipeline includes dividing the physical pixels into  $0.2''$  virtual ones, plus bias, flat field, and dark field corrections. After obtaining the astrometric information (Budavári et al. 2010), automated detections and measurements are conducted on the science images to the 2MASS calibration standard (Hewett et al. 2006; Hodgkin et al. 2009). This includes stellar astrometry in equatorial coordinates, aperture photometry with a set of aperture sizes, photometric

calibrations, and source classifications in terms of the probability of the source being a star (point-like) or galaxy (extended), or contaminated due to noise or saturated pixels. The overall classification of a source is obtained by combining independent probabilities of source classifications from individual-epoch images using Bayesian classification rules (Hambly et al. 2008). A “stellar” source has to have an overall probability of 90% or greater to be considered point-like. The detection tables of individual images were then merged to cross-match the detections of the same sources in different wavebands and at different epochs. The outcome is a table of all sources detected in the field with astrometry and  $JHK$  photometry, both time-averaged and by individual epochs, as well as source classifications. When a single time-averaged measurement of a star is needed, we use the astrometry and photometry based on the stacked mosaic image in the waveband of interest.

The pipeline-reduced measurements are available in the database WSERV9v20170222, from which we retrieved them via SQL inquiry. WSERV9 is a combined

<sup>7</sup> <http://wsa.roe.ac.uk/>

**Table 1**  
Observation Log

Epoch Order	Start Time (UTC)	Note
1	2014 Jul 18, 09:17:53	
2	2014 Jul 25, 12:36:29	
3	2014 Oct 06, 07:35:49	
4	2014 Oct 30, 04:32:44	
5	2014 Nov 06, 04:43:15	
6	2014 Nov 30, 05:39:27	
...	2015 Aug 05, 07:59:21	only first 2 positions in <i>J</i>
7	2015 Aug 07, 08:24:26	1 more run in <i>J</i>
8	2015 Aug 28, 08:08:53	
9	2016 May 24, 13:22:46	
10	2016 May 31, 12:21:16	
11	2016 Jun 02, 13:34:59	
...	2016 Jun 07, 13:54:34	only in <i>J</i>
12	2016 Jun 09, 13:26:30	
13	2016 Jun 10, 13:20:21	
14	2016 Jun 20, 11:50:20	
15	2016 Jun 23, 11:37:01	
16	2016 Jun 25, 13:25:27	
17	2016 Jun 26, 12:27:38	
18	2016 Jul 05, 11:09:59	
19	2016 Jul 08, 10:46:52	
20	2016 Jul 10, 10:34:21	
21	2016 Jul 12, 12:07:23	2 runs in each band

program made up of U/14B/UA16, U/15B/UA20 and U/16A/UA19 and the data were processed as a correlated multi-epoch project to produce contemporary colours in *JHK*, much like the WFCAMCAL data set described in Cross et al. (2009) or the Orion Nebula Cluster (Rice et al. 2015). The data can be made available by contacting Serena Kim (serena@as.arizona.edu).

### 2.3. Other data sets

We make use of a number of other data sets, as described in the Appendix.

### 2.4. The Extensive Catalog

In this work we are only interested in stellar sources with accurate photometry. To allow for systematic as well as statistical errors, we adopt 0.05 magnitude (signal-to-noise ratio  $S/N \gtrsim 20$ ) in the stacked all-epoch mosaic images in all three bands as the threshold of photometric uncertainty for inclusion in our study. This threshold rejects bright stars by the requirement of non-saturation and rejects faint stars by the maximum photometric error. A total of 111,657 qualified stars is found in the entire UKIRT/WFCAM field of view. We describe this list as the “extensive catalog” representing the largest set of stars with possibly useful measurements, which is not selected based on individual-image measurements or any time-domain information. The magnitude ranges in the extensive catalog are from 10.6 to 20.5 in *J*, 10.3 to 19.6 in *H*, and 9.9 to 19.3 in *K*. As a sample of the data products, Figure 1 shows the mosaic image of the Tr 37 in false color using deep stacked UKIRT/WFCAM images.

## 3. SELECTION OF STARS WITH HIGH QUALITY DATA

Not every star in the extensive catalog is suitable for variability analysis. Many of them have post-processing error flags from the pipeline at some epochs in some wavebands. These are warnings that the measurements

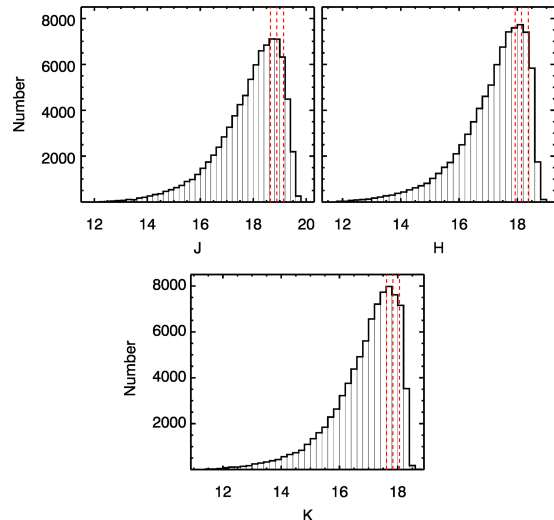


**Figure 2.** Histograms of the magnitude distribution of all detected stars in the *JHK* band variability catalog. In each plot, the red dashed lines, from right to left, label the brightness levels for 70%, 80%, and 90% of all detected stars.

in question may be biased or have other potentially significant data issues (Hodgkin et al. 2009). After visually inspecting many of these flagged stellar images, we find that the flags can arise from quite a few factors related to the observational conditions, such as close binaries resolved only during the best seeing conditions, slight focus inaccuracy, or high sky brightness at some epochs. Other than the flagged observations, some stars are simply undetected at some epochs, possibly because of unfavorable observational conditions. We assess the quality of individual photometric measurements by classifying a star at each epoch to either have a good observation, an error-flagged observation, or a missing observation. Only good observations are used to calculate the variability classifications.

Given that each star is covered by at least 24 images in *J* and 21 observations in *H* and *K*<sup>8</sup> (Table 1), we require a star to have at least 18 good observations in each of the three bands for its variability classification to be considered reliable. This threshold was set after examining sample light curves for sources with fewer good observations; 18 observations eliminated virtually all questionable cases. Additional tests of the method included plotting the possible variables as an image and adjusting the procedures to eliminate any suspicious spatial clustering (e.g., along the “seams” in our coverage at the extreme edges of the arrays). A total of 85,814 stars qualify, which make up our final catalog for the purpose of variability analysis, i.e. the “variability catalog,” which is a subset of the “extensive catalog.” The magnitude ranges in the final variability catalog are from 11.7 to 20.1 in *J*, 11.5 to 19.2 in *H*, and 11.2 to 18.7 in *K*. The magnitude histograms in each band are shown in Figure 2; the behavior suggests completeness limits of  $\sim 18.3$ , 17.7, and 17.4 respectively at *J*, *H*, and *K*. In this section, we describe the analyses conducted on this catalog to identify variable stars.

We assign one of five quality flags to each star in the

<sup>8</sup> Stars that lie in the narrow strips with overlapped coverage at consecutive dithers may be observed by a multiple of 24/21 times.

extensive catalog as described in Table 2. The variability catalog only includes stars with a quality flag  $\geq 1$ . It is likely that some stars with less than 18 good observations in at least one band (which thus are excluded from the variability catalog) may still be true variable stars. Although some of these stars are probably genuinely variable, many of these cases may have other causes such as asteroids or artifacts from bright stars. We do not consider their variability classifications further.

#### 4. ANALYSIS OF VARIABILITY

This section describes how we have combined two approaches to identifying variable stars from our “variability catalog”: (1) analysis of the rms fluctuations in the measurements of the stars; and (2) application of the Stetson Index that evaluates correlated variations in multiple photometric bands. Application of these two methods together leads to identification of 289 variable stars with K magnitude  $< 17$ , a sample that we analyze in the next section.

##### 4.1. Initial Variability Identification Through RMS Fluctuations

For each of the  $J, H, K$  bands, a set of statistics is calculated for each star in the catalog, including the mean, median, rms, minimum and maximum magnitudes, and skewness (Sesar et al. 2007; Cross et al. 2009), based on the photometry with the best aperture. The best aperture is defined as the aperture size that gives the lowest rms for the photometry of the object with the appropriate aperture corrections, an approach that yields better measurements in crowded regions than using a single, fixed aperture (Irwin et al. 2007; Cross et al. 2009). The means and rms’s for all sources are used to derive a fit to the expected scatter as a function of magnitude (e.g., Strateva et al. 2001), which we call the “expected rms” or  $xExpRms$ <sup>9</sup>. This gives the photometric uncertainty for band  $x$  ( $J, H,$  or  $K$ ) based on an individual image. For a non-variable star, this error should be an accurate estimate of the real scatter of the photometry in a time series, and is similar in principle to the error estimation in Hodgkin et al. (2009) as applied by Rice et al. (2012, 2015).

Variability is identified as in Cross et al. (2009), using attributes from the database. That is, the “expected rms” is subtracted, in quadrature, from the real rms scatter of the photometry at different epochs ( $xMagRms$ ). This reveals the variability of the star, in the form of “intrinsic rms ( $xIntRms$ ),” beyond the noise in the system. Specifically, in  $x$  band where  $x$  equals either  $J, H,$  or  $K$

$$xMagRms^2 = \frac{1}{xndof} \sum_{i=1}^{xndof} (x_i - xmeanMag)^2 \quad (1)$$

$$xIntRms = (xMagRms^2 - xExpRms^2)^{1/2} \quad (2)$$

where  $xndof$  is the number of good observations and  $xIntRms$  is the rms intrinsic variability, both defined in  $x$  band. To identify a star as a candidate for variability,

<sup>9</sup> We use the notation supplied with the pipeline products to expedite comparison with other UKIRT programs.

we require that the probability of the source being variable be  $> 0.9$  in each band, estimated by integrating the reduced  $\chi^2$  function:

$$xchiSqpd = \frac{1}{xndof - 1} \chi_x^2 = \frac{1}{xndof - 1} \sum_{i=1}^{xndof} \left( \frac{x_i - xmeanMag}{xExpRms} \right)^2 \quad (3)$$

$xchiSqpd$  is calculated under the null assumption of non-variability with the expected rms calculated above; for details see Cross et al. (2009).

We then conduct a second test on the candidate variables. We identify a star as a confirmed variable only if the weighted average ratio of the intrinsic to expected rms over all bands is greater than 3:

$$wsrms = \frac{\sum_{x=J,H,K} w_x \frac{xIntRms}{xExpRms}}{\sum_{x=J,H,K} w_x} \geq 3 \quad (4)$$

where the weight  $w_x$  is proportional to the number of good observations in each band; the band with the most observations has a weight  $w_x = 1$ .

There are 328 stars that pass both of these tests (we designate variables by VARCLASS = 1, with the remainder as VARCLASS = 0).

##### 4.2. Application of the Stetson Index

We used the Stetson Index,  $S$ , (Stetson 1996) as an alternative way to identify variable stars:

$$S = \frac{\sum_{i=1}^p g_i \operatorname{sgn}(P_i) \sqrt{|P_i|}}{\sum_{i=1}^p g_i} \quad (5)$$

Here,  $p$  is the number of pairs of simultaneous observations of a star,  $g_i$  is the weight of the  $i^{\text{th}}$  measurement, and  $P_i$  is the product of the normalized residuals of the two observations where the normalized residual of the  $i^{\text{th}}$  observation is

$$\delta_i = \sqrt{\frac{n}{n-1}} \frac{m_i - \bar{m}}{\sigma_i}, \quad (6)$$

where  $n$  is the number of observations in a band,  $m_i$  is the magnitude in the  $i^{\text{th}}$  observation,  $\sigma_i$  is the observational uncertainty in that observation, and  $\bar{m}$  is the average magnitude.

Nearly all of our observations provide simultaneous  $J, H,$  and  $K$  measurements of a source. We computed  $S$  for each pair of colors, i.e., three values for each source<sup>10</sup>. We then conducted a number of tests to determine the optimum way to utilize this information. First, considering the three indices separately might be important

<sup>10</sup> We deleted the most discordant of all repeated photometry of a star before the calculating Stetson index if it was made within  $\sim 50$  min from the previous one, roughly the time needed to complete one epoch. This removed double photometry of the stars at the edge of a field where the second telescope pointing resulted in a second measurement.

**Table 2**  
Definition of the Quality Flags for Time-domain Measurements

Quality	VarCat <sup>a</sup>	Criteria
2	Y	No post-processing errors in any band at any epoch (at least 21 “good” measurements in any band).
1	Y	At least 18 “good” measurements (without post-processing errors) in each of the <i>JHK</i> bands.
0	N	Less than 18 “good” measurements in at least one band.
-1	N	No reliable single-epoch photometry in at least one band.
-2	N	No minimum/maximum magnitude in at least one band (one or no good single-epoch photometry).

<sup>a</sup> “Y” if included in the variability catalog, “N” if not included.

if there are sources that vary significantly in two adjacent bands but not in the third. However, we found no convincing cases of such behavior from comparing the band-pair Stetson Indices. In addition, as discussed in the next section, there were in the end no examples of single-band variations that escaped notice in other ways. We therefore averaged the three values of  $S$  for each source. We found that these averages had a Gaussian distribution; assuming symmetry (i.e., that the number of false variability identifications can be deduced from the low side of the Gaussian), we found that  $S \geq 1$  is required to avoid false identifications fully (Rice et al. (2012, 2015), for example, adopted the same threshold). Since we do not know that the Gaussian is a perfect fit, we adopt this conservative criterion to identify variable stars purely through the Stetson index.

We adopted a different approach for sources where our  $\chi^2$  analysis indicated variations. Already the gaussian distribution indicates that  $S \geq 0.7$  indicates a probability  $< 0.1\%$  of a false identification of variability. We examined the light curves of sources with  $S > 0.5$  and found that those with  $S < 0.7$  frequently did not present convincing evidence for variations, but above this value most cases did imply variations, with the number of false identifications rapidly decreasing as  $S$  approached 1. Therefore, if a source was identified as a variable in the  $\chi^2$  analysis *and* had  $S \geq 0.7$  *and* also passed visual inspection as showing true variations, we accepted it as a true variable.

#### 4.3. Single-Band Variability

Both the  $\chi^2$  and Stetson Index approaches emphasize simultaneous variability in more than one spectral band. We carried out a third search in case there are variables that exceed the threshold for detection only in a single band and that were missed by these approaches. For example, a non-variable star with a highly dynamic dusty disk might show significant variability in  $K$  band because of the varying excess, but in  $J$  band where no significant excess is present, the star itself may not have detectable variations. Such a star might be disqualified by the all-band requirement.

Without the confirmation provided by variations in multiple bands, we need to be alert to possible spurious causes of variations. An example is a relatively low ratio of signal to noise. To probe this possibility, in each band we calculate the average and median flux densities, measured on the mosaic images in each band, of all identified variable stars in that band ( $xVARCLASS = 1$ ,

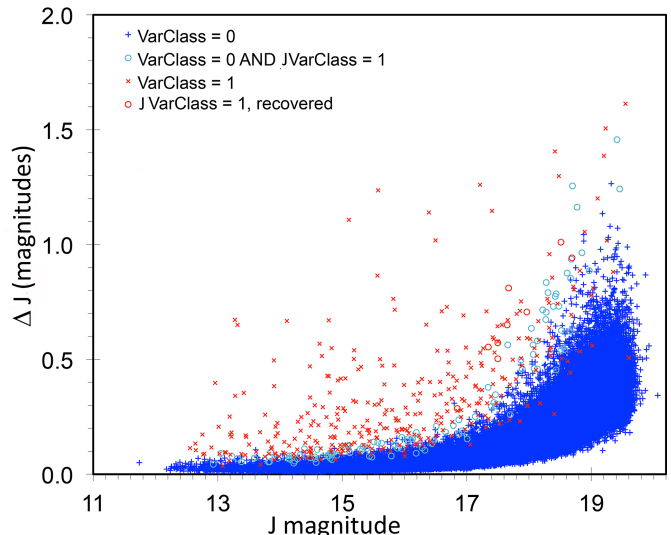


**Figure 3.** Peak-to-peak amplitude in magnitudes as a function of the mean  $J$  magnitude in the mosaic image. The points are colored to show the overall variables ( $VARCLASS = 1$ ) as red crosses. Single-band variables that do not qualify as overall variables ( $JVARCLASS = 1$  but  $VARCLASS = 0$ ) are marked with cyan circles, unless they have  $xchiSqpd \geq 20$  in that band, in which case they are plotted as red circles. Other non-overall variables are in blue. Stars with peak-to-peak amplitude higher than 2 mag are not shown. The stars indicated in red circles are candidates to add to the variable category; they are clearly differentiated from the distribution of non-variable stars (blue).

where  $x$  designates the band,  $J$ ,  $H$ , or  $K$ ) and compare them with those of the subset in which the stars are non-overall variables ( $VARCLASS = 0$ ). Although many of the single band variable candidates are faint, suggesting low signal to noise, there are a few that are bright enough that the variations might be real, as illustrated for the  $J$  band in Figure 3. We use the reduced  $\chi^2_{red}$ , or  $xchiSqpd$  (equation (3)), in a more stringent test to identify single-band variations. Given the possibility of false identifications, we have been conservative. A star is considered to vary if it is identified in any of the  $J, H, K$  bands with  $\chi^2_{red} \geq 20$  relative to the nominal measurement errors (given systematic noise of  $\sim 2\%$ , the significance is typically  $3 - 5\sigma$ ). This recovers 36 stars in total (11 stars by  $\chi^2_{red}$  in  $J$ , 6 in  $H$ , and 19 in  $K$ ). However a review of the individual  $JH, HK$ , and  $JK$  Stetson Indices and of the light curves of these objects led to the conclusion that no high-confidence variables had been added to our sample.

#### 4.4. Summary

In total, there are 359 stars with detected variations in our final “variability catalog”, an incidence of  $359/85814 = 0.42 \pm 0.02\%$  covering the full survey field. We will show that 1/3 of them are probable cluster members, implying that the identified variables among true field stars are  $\leq 0.3\%$ . This value can be compared with the detection of variability in  $\sim 1.6\%$  of the field stars with similar data by Wolk et al. (2013a) in a field at the same Galactic latitude and just 7 degrees away in Galactic longitude. The greater number of epochs in their monitoring might account in part for the higher detection rate, but with only four nights of observation Pietrukowicz et al. (2009) detected variability in 0.7% of field stars in Carina. The comparison indicates that our analysis is conservative and does not return a large number of false indications of variability. The lack of field star contamination is important for the analysis we will conduct on the sample in the following section (Section 5).

Figure 3 and similar statistics for  $H$  and  $K$  show where the distribution of variability amplitudes will begin to be biased against small amplitudes at faint limits. Analyzing this effect at  $K$  as the fiducial band for our study, the survey should be essentially unbiased in variability amplitude down to  $K \sim 16$ , will miss about the 20% of the smaller amplitude sources at 16.5, and will become increasingly incomplete in the smaller amplitude range below 17 mag. In addition, at faint limits it becomes increasingly difficult to identify faint nearby sources that might be responsible for false indications of variations due to the effects of seeing variations from night to night, and interference by the wings of the PSFs of nearby bright sources also becomes more likely. We therefore base the analysis of the variable source population only on sources with  $K < 17$ . Based on the color-magnitude diagram in Section 5.4, we find 121 possible cluster members among the variable sources. The Gaia DR2 parallaxes of two of these sources indicate they are foreground to the cluster. In addition, 63 of the apparently variable stars that appear to be non-members are fainter than  $K = 17$ . That is, the study is based on 119 variable probable cluster members with  $K < 17$ , listed in Table 3, that we will distinguish from 170 variable nonmembers based on placement on the CMD (Section 5.4).

Table 4 lists the variable stars that are nonmembers according to the CMD analysis; we include those fainter than  $K = 17$  but include them only as possible variables. Figure 4 shows the locations of the variable stars brighter than  $K = 17$  mag, differentiating probable cluster members from those that are probably in the field.

## 5. ANALYSIS

The Cep OB2 region, including IC 1396A and the surrounding clusters NGC 7160 and Tr 37, has been previously observed for YSO variability at other wavelengths. In the first subsection of this discussion, we compare known variable stars (from two studies, one in the  $R$  and  $I$  and the other in the *Spitzer* IRAC photometric bands) with our variability catalog. In the following subsection, we discuss the variability of the relatively bright Tr 37 cluster members identified by Sicilia-Aguilar et al. (2004, 2005, 2006b). In the next subsection, we carry out a similar study of the fainter sources from a different region

of the cluster identified by Sicilia-Aguilar et al. (2013). These subsections demonstrate that we detect variations in a large fraction ( $65 \pm 8\%$ ) of the *bona fide* cluster members. Therefore, in the following section we identify a homogeneous sample of cluster members on the basis of variability and a location on the  $K, I - K$  color-magnitude diagram that is consistent with cluster membership. This sample includes many newly identified members, in particular, faint ones. In the final subsections, we discuss the characteristics of the variability of individual cluster members from this sample that are of particular interest.

### 5.1. Previous Studies of Variability

In their Tables 6 and 7, Sicilia-Aguilar et al. (2004) gave variability identifications of stars in the region in the  $R$  and  $I$  bands. The two tables combined have 77 stars in total, 31 of which are within our UKIRT/WFCAM field of view and not saturated in any band. We cross match the 31 stars and find that 30 of them have counterparts within  $2''$  detected by UKIRT. The maximum matching distance is  $1.2''$ .<sup>11</sup> Among the 30 stars with stellar counterparts in our catalog, only nine probable members are in the variability catalog. Six of these nine are classified as overall variables: 11-2037, 11-2131, 14-1017, 11-383, 13-924, and 12-1091, in the nomenclature of Sicilia-Aguilar et al. (2004). (The 3 stars that we do not find variable in  $JHK$  are 12-1081, 12-1825, and 13-1161.) These stars are listed in Table 5 along with additional information about the variability of the bright cluster members.

We now turn to the mid-infrared. Morales-Calderón et al. (2009) found 41 stars to be variable out of a sample of 69 in the region in the *Spitzer* IRAC bands from 3.6 to 8.0  $\mu\text{m}$ , with 40% of the sample showing peak to peak amplitudes  $> 0.1$  mag. To explore this result, we evaluated the variations of the 41 stars listed in Morales-Calderón et al. (2009), Table 3. Although our observations are removed in time from those reported in this table, we can look at the type of the *Spitzer*-detected variability to compare with our results. Twenty five of the stars are within the parameters of our study - this excludes stars that are above our saturation limits in  $JHK$  and those that are so red that we would not have reliable  $I$  measurements and hence where we could not determine them to be cluster members based on the  $K, I - K$  color magnitude diagram (see Section 5.4). The distribution of peak-to-peak amplitudes in our study implies that we are relatively incomplete for amplitudes  $< 0.1 - 0.12$  mag, corresponding to RMS variations of  $\sim 0.03$  mag<sup>12</sup>. Assuming that the  $JHK$  variations should have similar sizes as those in the IRAC bands, we eliminate stars below this variability threshold, leaving 19. We have found variations in only five of these stars, i.e., 26%, of which only four are

<sup>11</sup> There is one star, 12-583 in Table 6 (Sicilia-Aguilar et al. 2004), that has no match in our catalog within  $3''$ . There is a source detected  $0.88''$  away, but it is classified as a galaxy (extended source) with very high confidence ( $P_{\text{galaxy}} = 0.999657$ ) by the pipeline (Hamby et al. 2008) and thus is excluded from our catalog. Nonetheless, Sicilia-Aguilar et al. (2010) indicate it is a star of spectral type M0; an inspection of the stacked image finds a tail of the source significantly extended to the east. Though a binary star is one of the possibilities, for data homogeneity we do not count any extended source identified by the WSA pipeline.

<sup>12</sup> Making the usual assumption that the peak-to-peak variation is four times the RMS one.

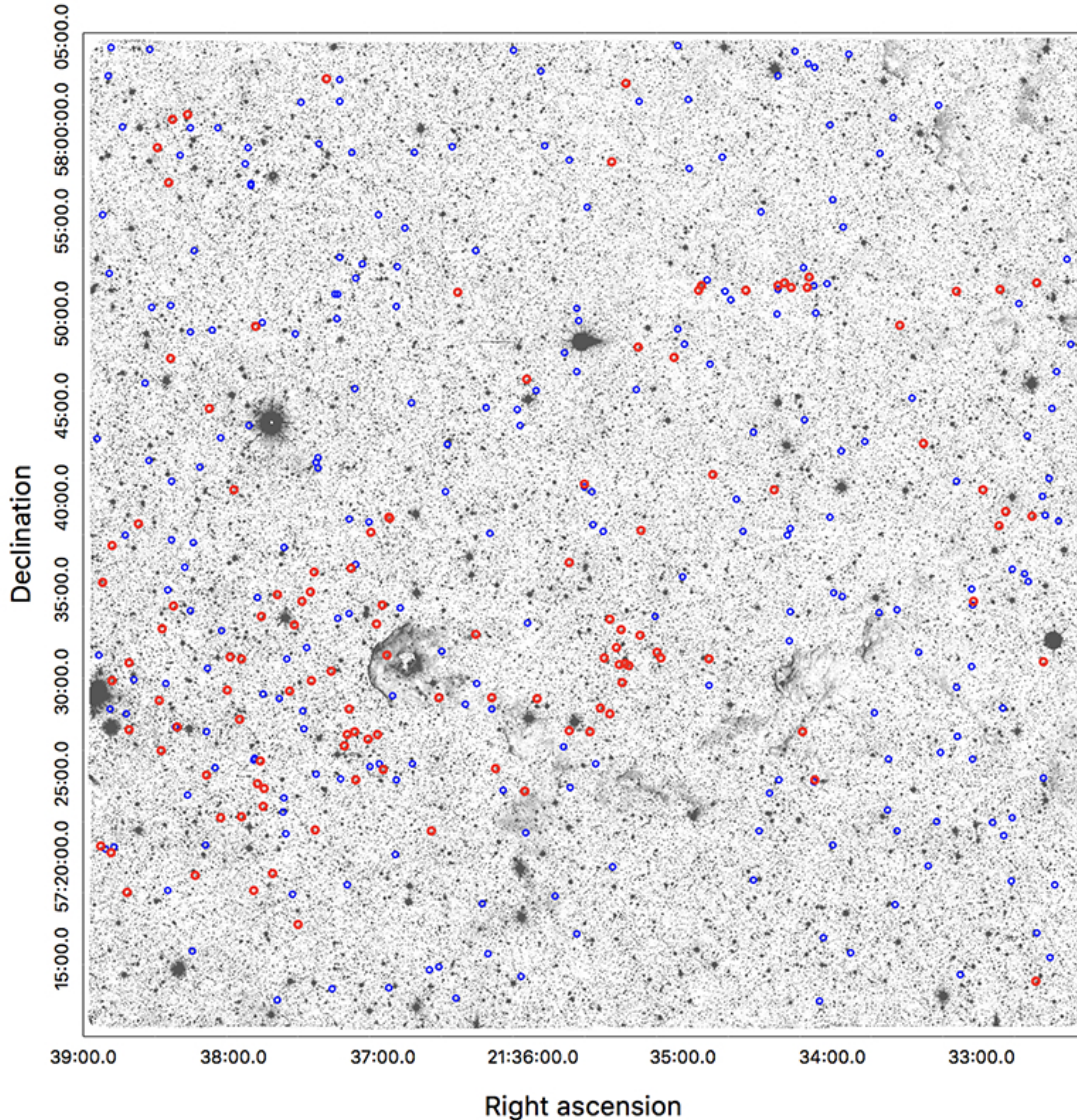


**Figure 4.** A UKIRT/WFCAM image of the surveyed region in  $K$  band. North is up and east is to the left; Variable cluster members are marked by magenta circles  $15''$  in radius. They tend to lie in the vicinity of IC 1396A. Small blue circles  $8''$  in radius mark additional variable stars; these stars are more uniformly spread over the field.

identified as variable by Morales-Calderón et al. (2009). Although nominally consistent with the 40% variability above 0.1 mag reported by Morales-Calderón et al. (2009), the comparison is surprising in the low rate of sources with variations seen in both wavelength ranges.

One explanation is that the emission mechanism in the IRAC bands is different from that in  $JHK$ , e.g., dominated by the photospheric variability, extinction changes, and accretion events onto the stellar surfaces at  $JHK$  and by circumstellar disk behavior in the IRAC bands. For example, two of the four variables from both studies (i.e., 182 & 192) appear to have  $JHK$  variability due to extinction variations (see Section 5.4). However, for the first the rms variations are the same size at [4.5] as at [3.6], which is not expected if the variations in these bands are also due to extinction; i.e., the variations seen by Morales-Calderón et al. (2009) are not of the same origin as those we find at  $JHK$ . Figure 5 examines this possibility more generally. The figure tests how many of

the IRAC variables may *not* have excesses in  $JHK$ . It shows the location on the  $J-H$  vs.  $H-K$  diagram of the IRAC variables, corrected for two possible levels of extinction,  $A_V = 1.3$  and 2, covering the range of plausible values for cluster members. These points are compared with the young stellar locus from Luhman et al. (2010). Six of the stars have colors compatible with stars of type  $\leq M6$  with no excess emission (one of these has rms variations  $< 0.03$  mag); two more have colors consistent with stars between  $M6$  and  $M8$  in type. At the same time, all of the sources have [3.6], [4.5], [5.8], and [8.0] colors consistent with Class II sources (Gutermuth et al. 2009). That is, a number of these sources indeed are likely to be dominated at  $JHK$  by photospheric emission and to have variable infrared excesses only in the IRAC bands.

Another possibility is that the lack of common variability arises in part because of the time interval between the observations; the *Spitzer* data used by Morales-Calderón et al. (2009) were obtained between January 24



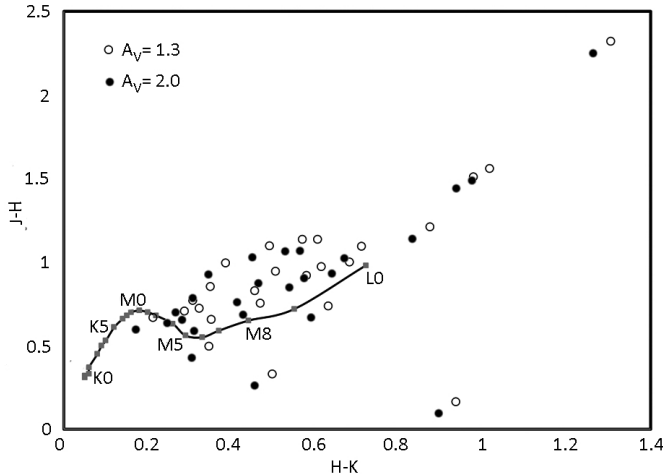


**Figure 5.** Placement of stars variable in the IRAC [3.6] and [4.5] bands (Morales-Calderón et al. 2009) on the  $J - H$ ,  $H - K$  color-color diagram. The locus of young low-mass stars and brown dwarfs is also shown, taken from Luhman et al. (2010). The filled dots are for  $A_V = 2$  and the open ones for  $A_V = 1.3$ .

and February 6, 2008, 7 to 9 years prior to our observations, and young star variability can be episodic over such time intervals (Audard et al. 2014).

### 5.2. Variability of Additional Members of Trumpler 37 from Sicilia-Aguilar et al. (2004, 2006b)

A series of papers led by Sicilia-Aguilar (Sicilia-Aguilar et al. 2004, 2006b; Sicilia-Aguilar et al. 2010; Sicilia-Aguilar et al. 2013; Sicilia-Aguilar et al. 2015) has used a combination of *Spitzer*, *Herschel*, and 2MASS infrared data, high resolution spectroscopy with *Hectochelle* on the MMT, and optical photometry to characterize about 160 sources in the Tr 37 field. Our survey for variability includes about 60% of this list, i.e., the 106 sources listed in Table 5. As discussed below, we gathered variability information for these sources in the  $r$  and  $i$  bands, from 2MASS at  $JHK$  in addition to our  $JHK$  survey, and from the ALLWISE  $W1$  and  $W2$  band measurements.

We have determined  $r$  and  $i$  variability from the IPHAS survey (Barentsen et al. 2014) on MJD 53,245, Pan-STARRS (Chambers et al. 2016) around MJD 55,990, and Sicilia-Aguilar et al. (2004). All of the measurements from IPHAS and Pan-STARRS were transformed onto a common system using linear fits with the  $r - i$  color as the independent variable. We then compared various sets, setting a conservative criterion for identifying that the source had varied: a discrepancy of  $\sim 0.15$  magnitudes (the value varied slightly from one data set to another) in both  $r$  and  $i$  and in the same direction. In addition, Sicilia-Aguilar et al. (2004) identify stars that varied in  $R$  and  $I$  over the 5 - 7 consecutive nights of data obtained in September, 2000, i.e., around MJD = 51,800. We characterize these variations as fast (F) and those between the different data sets, typically separated by years in time, as slow (S).

For our WFCAM data, we indicate detected variability as V and where none has been detected as N. The WFCAM saturates near magnitude 11.2 (in  $K$ ), so we cannot study variations of the brightest sources with it.

Tr 37 is among the regions scanned at longer integrations as the 2MASS all sky survey (Cutri et al. 2003) was being completed, producing measurements in the 2MASS

6X data base (Cutri et al. 2012). The all sky survey scanned the cluster on October 7, 2000 (MJD 51,824), the 6X survey surveyed 11 days later (MJD 51,835). We searched for variability between these two data sets as described in the Appendix. We have identified all of these variations as slow, since there is no indication of day-to-day behavior.

We also obtained data on these sources from WISE (Wright et al. 2010) in the  $W1$  ( $3.4 \mu\text{m}$ ) and  $W2$  ( $4.6 \mu\text{m}$ ) bands. There is a rapid cadence of these measurements from MJD 55,373 through 55,375, a few measurements on MJD 55,381, and another rapid series for MJD 55,553 through 55,555. Identification of variability within these data is discussed in the Appendix. Of the 29 sources with valid measurements from WISE and with coverage in our UKIRT monitoring in  $JHK$ , ten are variable in both spectral regions, a higher fraction than for the *Spitzer* monitoring reported by Morales-Calderón et al. (2009), despite the poorer sensitivity to variability with WISE. This result suggests that the low rate of overlap in variability in  $JHK$  and the IRAC sample of Morales-Calderón et al. (2009) may in part result from low-number statistics.

Table 5 includes additional information to assist with interpreting our results. We have used the ALLWISE  $W1 - W2$  color to search for sources with excesses. This color is only slightly affected by extinction, and the excesses tend to be large so we have not attempted to deredden it. Although the color baseline is small, the two colors are measured at the same time - an important consideration since most of the Tr 37 sources are variable. We have also indicated the accretion rates estimated by Sicilia-Aguilar et al. (2010). We indicate cluster membership, based on the spectroscopic survey in Sicilia-Aguilar et al. (2006b), where we have combined the indicators of membership into a single metric giving priority to radial velocities over the presence of emission lines<sup>13</sup> This priority is important because of the complexity of the line of sight toward Tr 37 and the likelihood that there are young stars projected onto the cluster that are not associated with it.

There are 78 stars from Table 5 that are both probable cluster members and have some information on variability. These 78 stars confirm expectations for relations among the different observational parameters. For example, 50 of these stars have measurements of accretion, of which 16 have accretion at a significant level (Sicilia-Aguilar et al. 2010). All 13 of these 16 stars with adequate variability data are also found to vary in one or more of the three wavelength regions in the table, and all 13 with valid WISE data have excesses above the stellar photospheric color in  $W1 - W2$ . Of the stars with variability information in  $JHK$ , 40/60 or 67% have been observed to vary. However, one of these stars is a possible foreground object (see footnotes to table) leaving the fraction of cluster members observed to vary at 40/59 = 68%. For all 78, about 2/3 have been observed to vary in one band or another, and about 1/2 have  $W1 - W2$  excesses (of those where we can measure them, omit-

<sup>13</sup> Specifically, we have indicated Y(e) as P, Y(r) as Y, P(r) as P, P(e) as P, Y(e)N(r) as PN, Y(e)P(r) as Y, Y(e)PN(r) as P:, and P(e)N(R) as PN, where the first designation is from Sicilia-Aguilar et al. (2006b).

ting ones in confused regions). These numbers imply that variability can produce identifications as complete as those based on infrared excesses, although we have used a relatively large number of epochs and bands and smaller-scale studies of variability will be less complete.

### 5.3. Variability of Lower-Mass Tr 37 Members from Sicilia-Aguilar et al. (2013)

Sicilia-Aguilar et al. (2013) extended their previous work to fainter stars, providing a list of members of Tr 37 down to the mid-M-star spectral type (e.g., covering most objects of stellar but not so faint as to be of brown dwarf mass). Identifying low-mass members of Tr 37 has been challenging because it is projected onto a rich field of stars; there are more than 100,000 stars detected within our UKIRT survey. Sicilia-Aguilar et al. (2013) addressed this issue by complementing isochrone models and optical color-magnitude diagrams with infrared excesses to select pre-main sequence candidates. They gave priority in their spectroscopic observations to the infrared excess sources, resulting in a possible bias toward such stars in their sample. Although the initial selection in Sicilia-Aguilar et al. (2013) sampled M type stars, their confirming spectroscopy (spectra obtained with Hectospec on the Multiple Mirror Telescope (MMT)) did not go as deep as very low mass late M stars/brown dwarfs. The confirmation rate for the sources with infrared excesses was high ( $\sim 90\%$ ), but it was much lower (5 - 20 %) for those without excesses; the sample is therefore largely selected on the basis of having circumstellar disks. Table 6 lists the sources in Sicilia-Aguilar et al. (2013) with valid variability observations (i.e., in our variability catalog). One of these stars, S13-081, appears to be foreground to the cluster according to its Gaia parallax. Thus, of the cluster members, 19/32, or 59%, are variable in our data. If we combine this result with those in Sections 5.1 and 5.2, the incidence of sources with detected JHK variability is  $65/100 = 65 \pm 8\%$ . In the following section, we use variability as a means to identify additional faint cluster members.

### 5.4. New Variable Member Candidates - Color-Magnitude Diagram Analysis

Variability is an alternative indicator of cluster membership that can be applied to very faint detection limits. We demonstrated in the preceding subsections that  $\sim 65\%$  of the cluster members are detected to vary in our survey. This result is placed in context in Figure 6; roughly, the percentage of variables identified in a cluster increases logarithmically with the number of epochs of observation. Our result is a bit above the overall trend and is consistent with up to  $\sim 80\%$  of the cluster members being variable, to be revealed with a sufficiently large number of epochs of observation. Although these statistics give a measure of the incompleteness that will result (i.e., about 35%), we have an adequate set of observations to identify members down to the brown dwarf regime (late M at the age of Tr 37). Selection of members on this basis should provide an incomplete but unbiased sampling of the cluster membership for sources fainter than our maximum brightness limits of 11.7 in *J*, 11.5 in *H*, and 11.2 in *K*. Given the extinction and relevant range of spectral types, the meaningful brightness limit

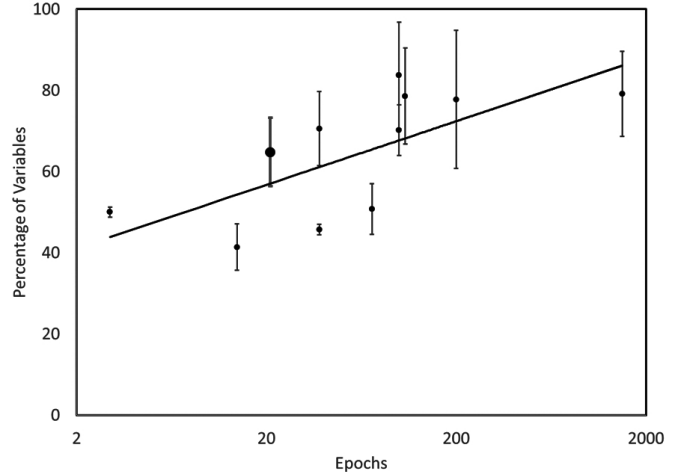


**Figure 6.** Percentage of cluster members identified as variables vs. number of epochs of observation. Data are in order of increasing epochs, from Megeath et al. (2012); de Oliveira & Casali (2008); Carpenter et al. (2001); Wolk et al. (2018); Rebull et al. (2015); Wolk et al. (2013a); Poppenhaeger et al. (2015); Günther et al. (2014); Flaherty et al. (2016); Parks et al. (2014). The value from this work is shown as the large dot with heavy error bars.

is 11.2 at *K*; cluster members of this brightness will fall below the limits at *J* and *H*. The completeness limits at *K* can be determined from the distribution of variability range in the identified variable sources and the rms noise as a function of *K* magnitude. The completeness corrections from the identified variables to the total over the range for the brighter sources are negligible for  $K < 16$  and are  $< 20\%$  for  $K < 16.5$ .

However, some of the variable stars in the survey may not be members of Tr 37. We will therefore use a color-magnitude diagram (CMD) to distinguish variable stars likely to be members from variable interlopers. The applications of CMDs to other young clusters have established where YSOs should locate in the diagram. In this work, we compare the CMD of Tr 37 with that of IC 348 (Luhman et al. 2003, 2016) for two reasons. First, IC 348 and Tr 37 are thought to be similar in age ( $\sim 3$  Myr, Herbst 2008; Sicilia-Aguilar et al. 2005), so their member stars should fall along similar loci. Second, IC 348 is much closer ( $311 \pm 32$  pc (Boyce et al. 2019) vs.  $945^{+90}_{-73}$  pc (Sicilia-Aguilar et al. 2019)) than Tr 37, with members known down to brown dwarfs. Our UKIRT data on Tr 37 are significantly deeper than the available data on IC 348 and reach a similar range of absolute magnitudes, providing a good comparison.

The CMDs of IC 348 were recently discussed in detail by Luhman et al. (2016) based on UKIDSS and CFHT *IZY* band data and the 2MASS data in *K<sub>S</sub>* band. Since our new UKIRT data are in *JHK* bands only, for direct comparison we adopt the optical photometry from the Pan-STARRS DR1 catalog (Chambers et al. 2016), which, like our photometry on the mosaic images, averages over a number of epochs. For comparison with the IC 348 CMD, we convert the Pan-STARRS *i* and *z* magnitudes to *I* as described in the Appendix. We plot all the spectroscopically confirmed Tr 37 member stars from Sicilia-Aguilar et al. (2013) together with the IC 348 members from Luhman et al. (2016) in the same CMD (Figure 7).

We will use the CMD to identify variable stars that

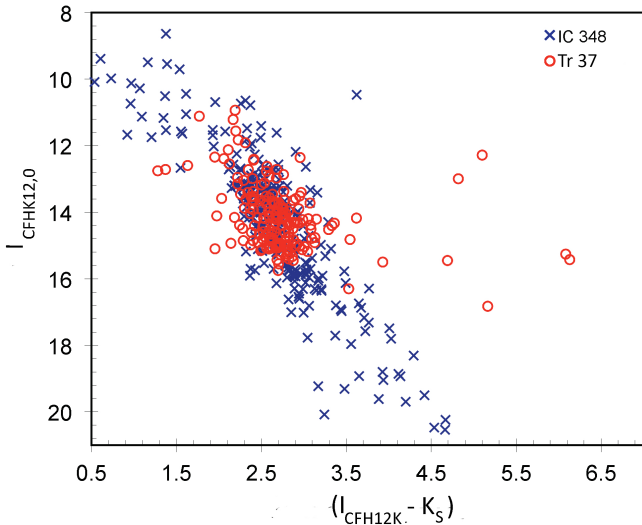


**Figure 7.**  $I, I-K$  color-magnitude diagram for all the high probability Tr 37 cluster members from Sicilia-Aguilar et al. (2013), superimposed on the CMD for IC 348 from Luhman et al. (2016). The values for IC 348 have been shifted fainter by 2.0620 mag.

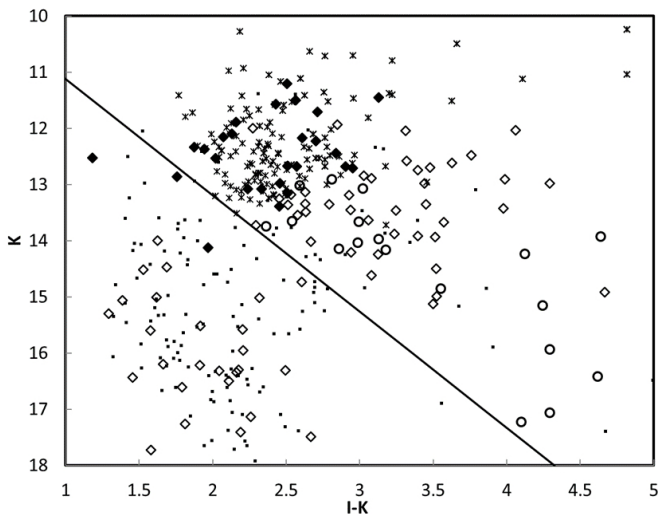


**Figure 8.**  $I, I-K$  color-magnitude diagram. The asterisks are for all the high probability Tr 37 cluster members from Sicilia-Aguilar et al. (2006b). The filled diamonds are for variable stars discovered in this work and with high weight ( $\text{SNR} > 10$ ) Gaia DR2 parallaxes indicating cluster membership. The open diamonds are similar except that they have low weight Gaia parallaxes ( $\text{SNR} > 2$ ) that are consistent with cluster membership. The small dots are sources where the parallaxes are inconsistent with cluster membership. The open circles are stars without measured parallaxes that we have assigned cluster membership based on their positions on the CMD. The diagonal line is the expected boundary between members and non-members; it has been determined to have the same slope and to be placed similarly relative to the cluster members as in Luhman et al. (2016).

could be members of Tr 37. We separated the locus of possible cluster members from that for background stars in analogy with the approach for IC 348 by Luhman et al. (2016). In Figure 8, we show the CMD for our variable stars with a dividing line placed to be analogous to that used by Luhman et al. (2016). The behavior of the high-probability cluster members from Sicilia-Aguilar et al. (2006b) causes us to conclude that most stars above the line are likely to be members. However, we tested

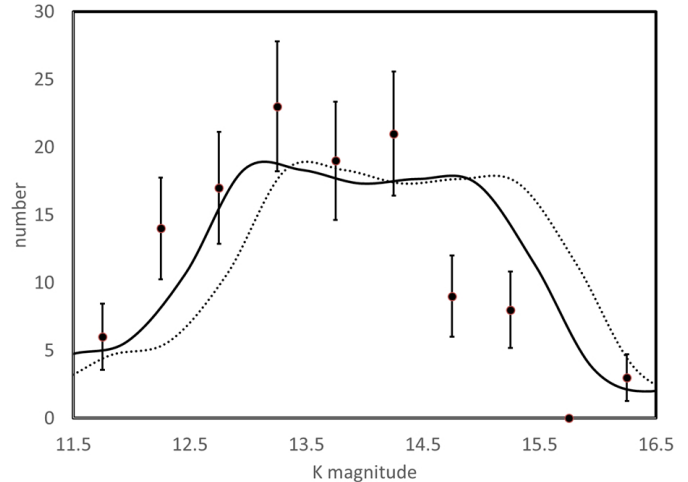


**Figure 9.** The  $K$ -band luminosity function for IC 348 (Muench et al. 2003) adjusted to the distance of Tr 37 (dotted line), based on Gaia DR2 parallaxes for both clusters, and compared with the  $K$ -band distribution of the sample of variable members of Tr37 (points with error bars). The values for Tr37 are not corrected for extinction, which would move them  $\sim 0.11 - 0.15$  magnitudes brighter (this correction has not been made to display the results over the range directly demonstrated not to suffer from biases due to saturation or incompleteness). As shown by the solid line, the fit is significantly improved by shifting the IC 348 luminosity function 0.36 magnitudes brighter, suggesting that the population in Tr37 is somewhat younger than that in IC 348.

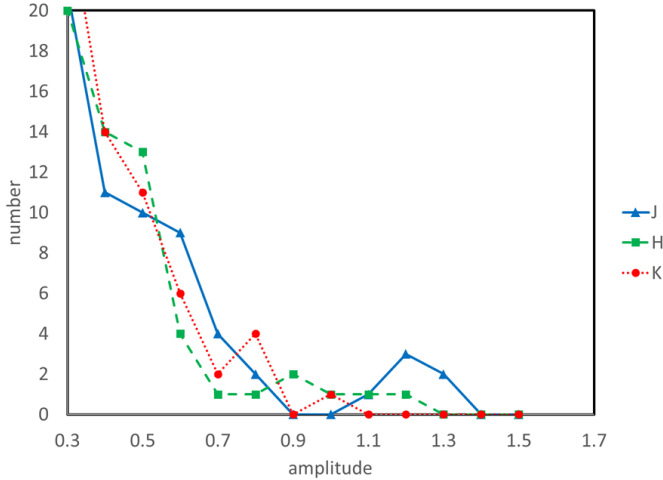
all candidate members against Gaia DR2 parallaxes and rejected two as being probable foreground stars. There are 16 stars that meet our criteria for cluster membership but do not have parallax measurements: given the small number of foreground stars among the stars with parallaxes, it is not likely that any of these stars are foreground. We therefore accept the sources above this line (except the two with large parallaxes) as possible members. The resulting 119 candidate variable cluster members are listed in Table 3, along with their numbers in the membership lists compiled by Errmann et al. (2013) and whether they are listed by Sicilia-Aguilar et al. (2013). This sample is likely to be about 2/3 complete and, based on the small fraction of field stars that are variable in our data, to have very low contamination.

Table 4 lists the additional variable stars that did not pass our tests for cluster membership.

### 5.5. $K$ -band luminosity function and CMD Comparison

Figure 9 shows the expected  $K$ -band luminosity function for Tr 37 based on that of IC 348 (Muench et al. 2003) adjusted for the relative distance of the two clusters. The similar ages would suggest that the luminosity functions should be similar and indeed they have similar shapes, but the best fit finds that the function is shifted significantly brighter for Tr37. To quantify this effect, we have shifted the luminosity function to minimize  $\chi^2$ , which occurs at a shift of 0.36 magnitudes, or at  $\sim 0.5$  magnitudes if we make a correction for extinction.

This conclusion can be tested by comparing the two clusters on the CMD. If the two clusters have similar ages, their members would be expected to locate around the same locus. We make a linear fit for the locus of IC 348 and use the same fixed slope to force a fit to the members of Tr 37. The difference in the intercept,  $2.06 \pm 0.36$ , is the *relative* distance modulus from isochrone fitting.



**Figure 10.** Peak-to-peak variability of the 119 probable cluster members for  $J$ ,  $H$ , and  $K$  bands. There are more highly variable sources (amplitude  $> 0.9$  mag) at  $J$  and  $H$  than at  $K$ .

However, the Gaia parallaxes indicate that the true distance modulus is about 0.36 mag greater than this value, agreeing qualitatively with the shift estimated from the luminosity function (before the additional correction for extinction).

The shift in the  $K$  luminosity function has the greater weight over the CMD because of its smaller dependence on extinction; nonetheless, the shift becomes about 0.5 magnitudes with the extinction correction for Tr37. The nominal errors in the Gaia-estimated distance (Sicilia-Aguilar et al. 2019) are too small to explain these shifts. However, there is evidence for a small bias toward underestimating parallaxes in Gaia (see summary in Xu et al. 2019). A weighted average of all the measurements (Xu et al. 2019) yields  $-53 \pm 3 \mu\text{as}$ , but this value is strongly influenced by the single input with the smallest quoted error. The average omitting this value is  $-56 \pm 11 \mu\text{as}$ . If we adopt  $-55 \mu\text{as}$ , the relative distance modulus between IC 348 and Tr37 is reduced by 0.11 mag with a 95% confidence error of about  $\pm 0.3$  mag, i.e., to account for the 0.5 mag shift in the  $K$  luminosity function would require that the distance be overestimated by an amount that is outside the expected errors. The behavior suggests that the  $K$ - and  $M$ -stars in our sample, which dominate the luminosity function, are somewhat younger than similar stars in IC 348. Our variability-selected sample is centered around IC 1396A (see Figure 4), so a plausible explanation is that many of these stars are associated with a population that is younger than typical for Tr37, e.g., the very young stars ( $\sim 1$  Myr old) discussed by Getman et al. (2012).

### 5.6. Characteristics of Individual Sources

This section illustrates the variability patterns of individual sources. By necessity, we focus on those with relatively large amplitude variations so that the patterns emerge clearly. This criterion will tend to omit stars that vary because of cool spots but should include the other previously identified types of variables (Wolk et al. 2013a,b). We should detect many periodic variables (Rice et al. 2012, 2015), although the low cadence of our observations will keep us from identifying them as such.

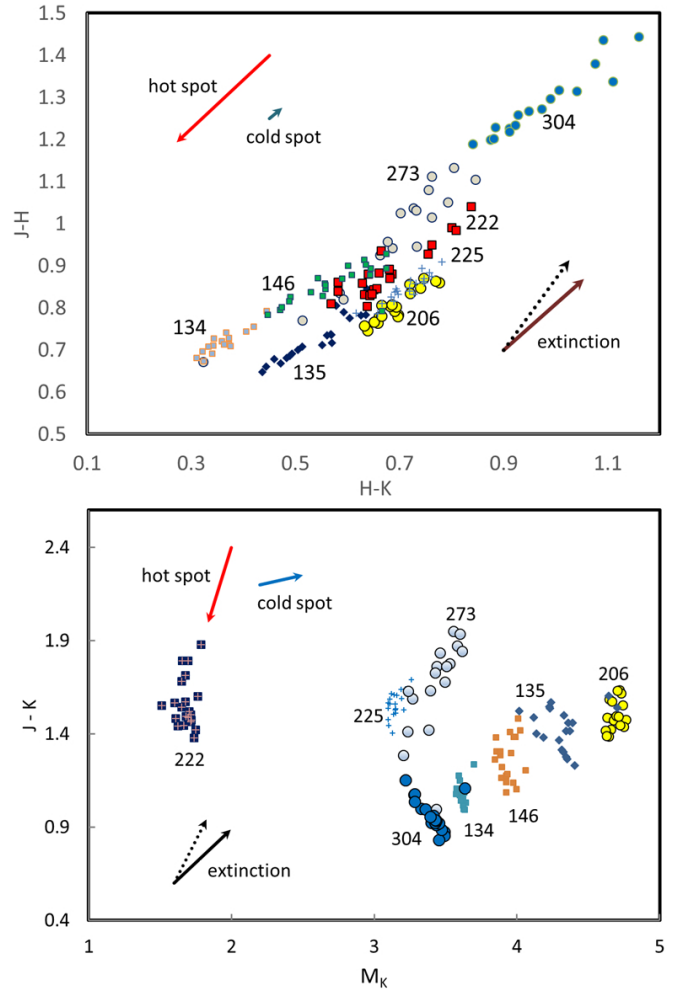


**Figure 11.** The  $J - H$ ,  $H - K$  color-color diagram (CCD) and  $J - K$ ,  $M_K$  color magnitude diagram (CMD) for sources where the change in  $J$  is large, but there is relatively little change at  $K$ . The behavior of a source acquiring a hot or cold spot is shown at the upper left with a red or blue arrow, respectively. The behavior due to changes in extinction is shown in the lower right of the CCD and lower left of the CMD, with a dotted line for standard interstellar behavior ( $A_V = 2$ ) and a solid line for an extinction law as expected for large grains (shown to be characteristic of the variable extinction in these sources in Section 5.6.3). The behavior of these sources suggests the presence of accretion hot spots, which are well above the temperature of the stellar photosphere and thus produce a large change at the shorter wavelengths when they rotate into view.

#### 5.6.1. Accretion hot spots on the stellar surface

This section discusses the sources whose behavior indicates accretion hot spots, based both on the color behavior of the variations, their chaotic nature, and the placement if the sources along the classical T Tau locus in the  $J - H$ ,  $H - K$  color-color diagram. Figure 10 shows that more cluster members have a high degree of variability in  $J$  than do in  $H$  or  $K$ . As shown in Figure 11, these objects also tend to have substantial scatter in the  $J - H$ ,  $H - K$  diagram. Light curves for two examples can be found in Figure 12. These objects potentially change output because of the appearance of a hot spot due to localized accretion onto the stellar surface (e.g., Wolk et al. 2013b). To provide a specific example, we have used the high flux level for source 222 on MJD = 56,960.192 and the low one a week later, on

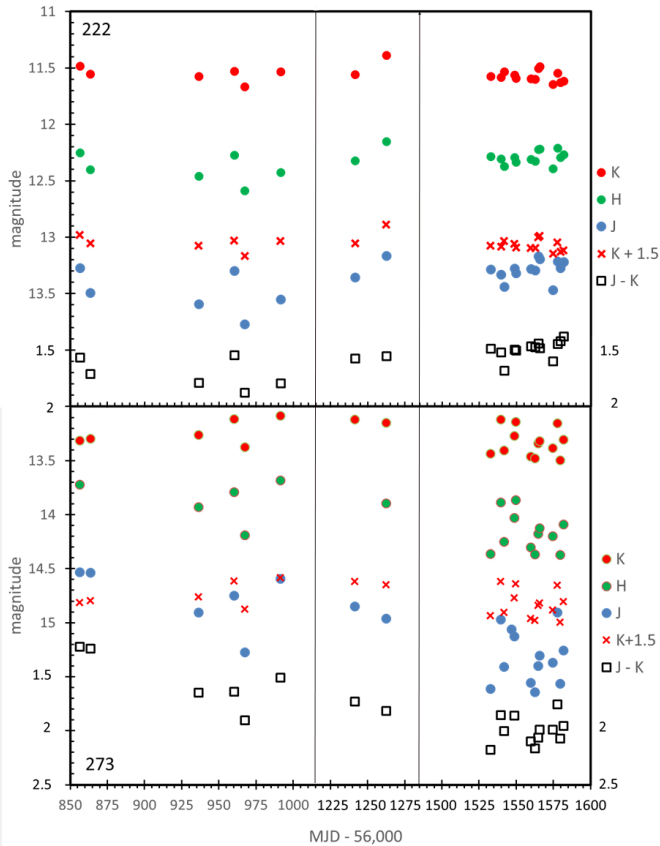


**Figure 12.** The light curves for sources 222 and 273, two of the most variable sources where the amplitude at  $J$  is  $>$  twice as large as that at  $K$ . The light curves have been compressed by eliminating epochs with no data, indicated by the light vertical lines. The data at  $K$  are repeated 1.5 magnitudes fainter to facilitate comparison with the  $J$  lightcurve. Comparison of the shifted  $K$  curve and the  $J$  one, and also the  $J-K$  color, show that the sources become bluer when they are brighter, i.e., the variations are driven by relatively large increases in the output at  $J$ .

MJD 56,967.20. We have dereddened the  $JHK$  measurements for  $A_V = 1.3$ , the average value for the cluster (Errmann et al. 2013), converted the resulting magnitudes to flux densities, and then subtracted the values for MJD 56,960.19 (low) from those for MJD 56,967.20 (high) to provide three photometric points for the difference, which we can ascribe to the variable component. Any fits are very degenerate; for example, we find that the photometry in the low state can be fitted well by a blackbody of 1950K, and to fit the high state we need to assume a coverage of 1.2% of its surface by a hot spot at 5200K. This calculation is used to generate the hot spot vector in Figure 11. If we increase the extinction by a factor of 3 to  $A_V = 3.9$ , the temperatures become 2500K and 9000K, respectively. The latter two values are reasonably representative of the photospheric temperature of low mass pre-main-sequence stars with hot spots observed in other studies, e.g., Wolk et al. (2013b)<sup>14</sup>. The rapidity of some of the variations (e.g., source 273) may result from hot spots rotating in or out of sight. Four of these sources, numbers 174, 222, 273, and 304, have been studied previously and the latter three have been

<sup>14</sup> In the following section we will identify some sources with dramatic rapid variations that change relatively little in near infrared color.

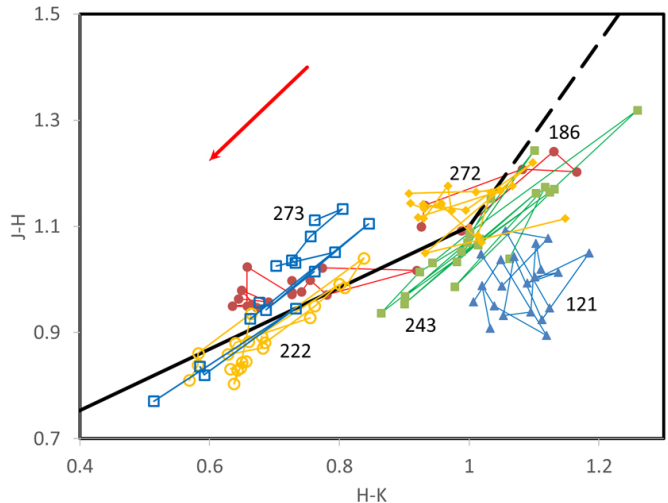


**Figure 13.** The behavior of the two hot-spot prototypes numbers 222 and 273, and four EXor-like sources, 121, 186, 243, and 272 on the  $J-H$ ,  $H-K$  diagram. The red arrow at the upper left is the expected vector for a hot spot and the black line (solid and dashed) is the CTTS locus from Meyer et al. (1997). Sources 222 and 273 follow the CTTS locus with moderate scatter, supporting the hypothesis that their variations arise primarily due to episodic accretion events onto the stellar surfaces, i.e., hot spots. The EXor candidates have a more chaotic behavior and more extreme colors.

found to have strong  $H\alpha$  emission (Nakano et al. 2012; Sicilia-Aguilar et al. 2013), consistent with the suggestion that their variability is associated with accretion, e.g., hot spots. Fig 13 shows sources 222 and 273 on the  $H-K$ ,  $J-H$  color-color diagram, along with the classical T Tauri Star (CTTS) locus (Meyer et al. 1997). The behavior of lying close to this locus throughout their variations indicates that these two sources are experiencing high and variable mass accretion and have similar accretion disk geometries (i.e., inner hole radii) to CTTS's in general (Meyer et al. 1997).

To complement the hot spot vector in Figure 11, we show the vector for normal interstellar reddening (Rieke & Lebofsky 1985) and for reddening by large grains (Steenman & Thé 1989). Extinction will be discussed further in Section 5.6.3. We also show the expected behavior for cold spots (Wolk et al. 2013b). These vectors show that in the  $J-H$ ,  $H-K$  diagram, the behavior of hot spot variations may be difficult to distinguish from extinction changes, but the  $J-K$ ,  $M_K$  diagram is more diagnostic, particularly relative to extinction by large grains, which we show in Section 5.6.3 is common around young stars.

### 5.6.2. Chaotic variability and EXors

Some of the most extreme variability patterns and amplitudes resemble those of EXor type objects (named after EX Lupi); four examples are sources 121, 186, 243, and 272 (Figure 14 and Figure 15). The amplitudes of these objects are similar to those of, e.g., sources 222 and 273, but their changes seem to be subject to more chaotic behavior and longer term trends. EXors show eruptive variability caused by rapid accretion rate changes by orders of magnitude (see Herbig 1998 and Audard et al. 2014 for review), and show smaller amplitude variability with more frequent outburst episodes compared with the related FU Ori type objects; the latter show much

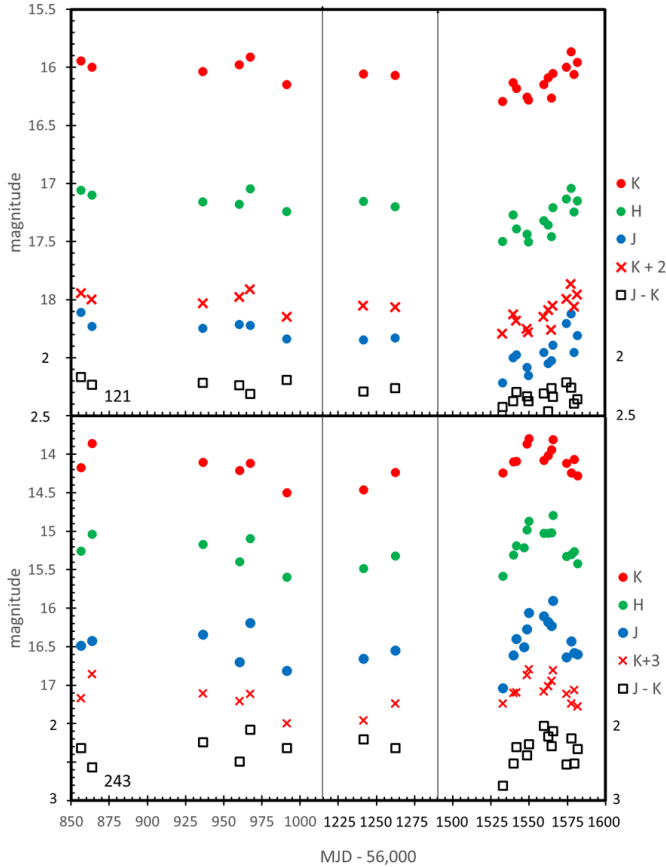


**Figure 14.** The light curves for sources 121 and 243 compressed as in Figure 12. Source 121 has fluctuations that are relatively similar in amplitude at all the bands, whereas source 243 has variations driven by increases in the output at  $J$  as indicated by it becoming bluer when it is bright.

larger variability ( $\Delta V \gtrsim 4$  mag) that can last for several decades. Frequent variability episodes of EXOrs are likely related to magnetospheric accretion of circumstellar disk materials onto the young star, which show higher amplitude variability at shorter wavelengths. Giannini et al. (2016, 2017) show multi-wavelength variability for an EXOr, V1118 Ori; we reproduce their data in Figure 16 showing the 2015 - 2016 outburst of this star, for comparison with the variations of Sources 121, 186, 243, and 272. The variability patterns of V1118 Ori and our sources 121, 186, and 243 are similar with a higher  $J$  band variability amplitude than in  $H$  and  $K$  band; for source 272, the changes are more similar in amplitude across the three bands. Peak to peak variability amplitudes of source 121 are 0.61, 0.46, and 0.43, for source 186 they are 1.13 mag, 0.99 mag, and 0.73 mag, for source 243 they are 1.14 mag, 0.8 mag, and 0.7 mag, and for source 272 they are 1.10 mag, 1.13 mag and 0.98 mag in  $J$ ,  $H$ , and  $K$  band respectively. In all four cases, the variations have trends with month- or year-long time scales, consistent with EXOr behavior (Audard et al. 2014). Source 186 shows in Figure 15 a different pattern than sources 121, 243, and 272, namely a general brightening with modest variations otherwise. Although this behavior is still consistent with being an EXOr, it could also arise through removal of obscuring materials along the line of sight (after MJD 57,500).

These four sources are shown on the  $H - K$ ,  $J - H$

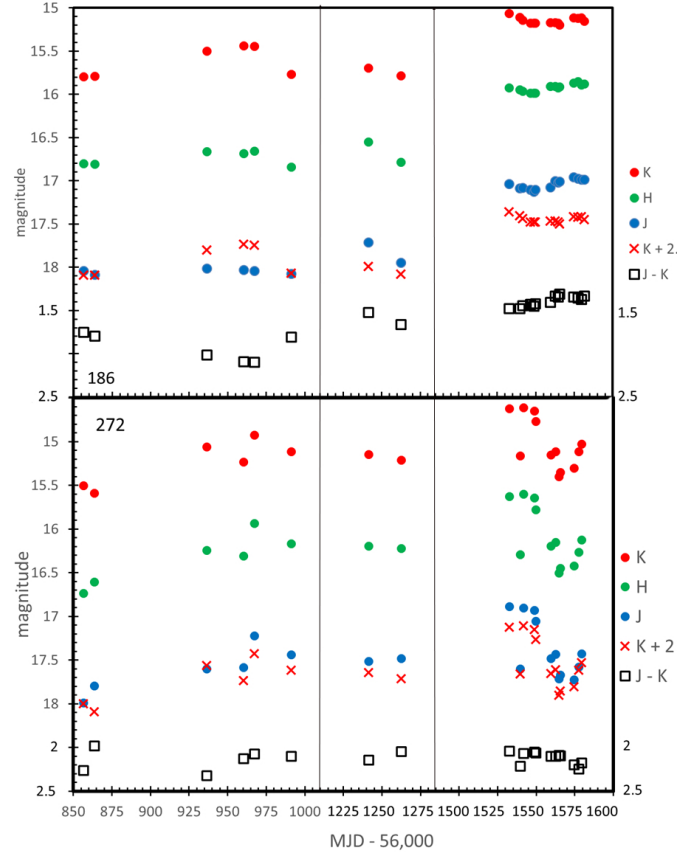


**Figure 15.** The light curves for sources 186 and 272 compressed as in Figure 12. Source 186 became significantly bluer after its transition to a relatively steady bright state. The colors of Source 272 are relatively unchanged through its variations.

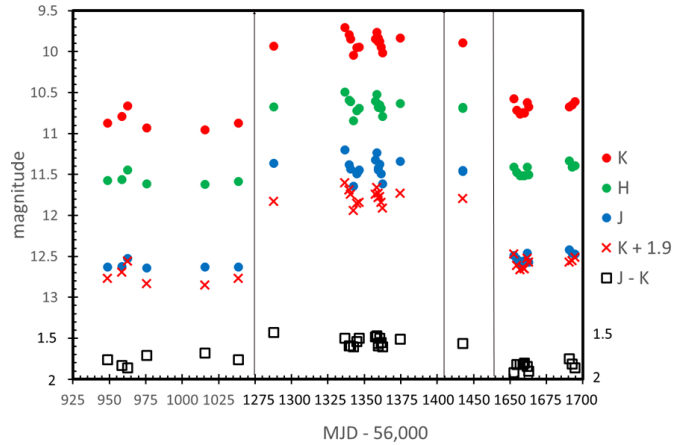


**Figure 16.** The light curve of V1118 Ori through its outburst in 2015 - 2016, compressed as in Figure 12, from Giannini et al. (2016, 2017). Its dramatic outburst results in a near infrared color only slightly bluer than when it is at a lower state, a situation similar to some of the EXOr-like sources in Tr 37.

diagram in Figure 13. Their extreme nature is confirmed by their passing into the protostellar disk regime to the right of the CTTS locus.

Another set of sources show chaotic variations but with smaller amplitudes (0.3 - 0.4 mag); we term these chaotic variables. Examples are numbers 72, 76, 157, 166, 232, 251, and 252. Their behavior might, for example, result from minor accretion events, or from a combination of

effects, such as both hot spots and variations of extinction (see following subsection). In such cases our simple categorization would not be definitive.

### 5.6.3. Large grains in circumstellar disks

Some sources appear to vary due to changes in extinction caused by grains larger than those typical of interstellar dust. Figure 17 shows color-magnitude and color-color diagrams for eleven sources with this behavior. We suggest that the variability in these sources is driven primarily by the intervention of clumps or other structures in their circumstellar disks (Rice et al. 2015; Stauffer et al. 2015). The large-grain vectors are based on the work of Steenman & Thé (1989), who showed that a simple extinction model with lower and upper size limits on the grains of 0.005 and 0.22  $\mu\text{m}$ , respectively, and with a size distribution of  $n(a) \propto a^{-3.5}$ , gives a good fit to the normal extinction law and then explored the changes resulting from an increase in the upper size limit. The solid black vectors shown in Figure 17 are from their calculation for a ratio of total to selective extinction,  $R = 5.9$ , corresponding to an upper size limit of  $\sim 1 \mu\text{m}$ .

We expect that extinction will result in a well-determined linear relation between  $J - H$  and  $H - K$  with minimal scatter around this trend as the extinction varies. We use this expectation to separate the sources into ones that obey this expectation and those that have larger scatter. To identify candidates where the variations might be dominated by variable extinction, we set the slope in  $(H - K)$  vs.  $(J - H)$  equal to the median for the sources in this part of our study, 0.77, and then minimized the reduced  $\chi^2$  for a linear fit to the data, with results as shown in Figure 18. We examined the sources in the intermediate zone, with values of  $\sim 2 - 4$  individually, and rejected those with anomalous behavior in the  $M_K$  vs.  $(J - K)$  diagram, typically ones with small slopes with large scatter, and those with relatively small variations. The sources with behavior possibly dominated by extinction are shown in blue in Figure 18 and the remaining ones in orange. Although our procedures to distinguish hot spot variations from extinction ones might just have separated sources with different slopes in the  $(H - K)$  vs.  $(J - H)$  diagram, Figure 18 demonstrates that, instead, it separates sources with small scatter around the linear trend from those with large scatter.

Changes in the minimum grain size have little effect on the relative extinction in the  $JHK$  bands (Steenman & Thé 1991), in agreement with expectations since the minimum size of typical interstellar grains is far smaller than the wavelengths of these bands. This situation underlies the independence of the  $JHK$  extinction law on the selective extinction ratio,  $R_V = E(B - V)/A_V$  (Cardelli et al. 1989). The behavior of the sources in Figure 17 and as summarized in Table 7 therefore suggests that the dust grains responsible for the extinction have a larger maximum size than those in the general interstellar medium, i.e. in agreement with other indications that in these protoplanetary disks significant grain growth has occurred.

### 5.6.4. Possible eclipses

Figure 19 shows the relevant parts of the light curves of two sources where eclipses are a possibility. Other

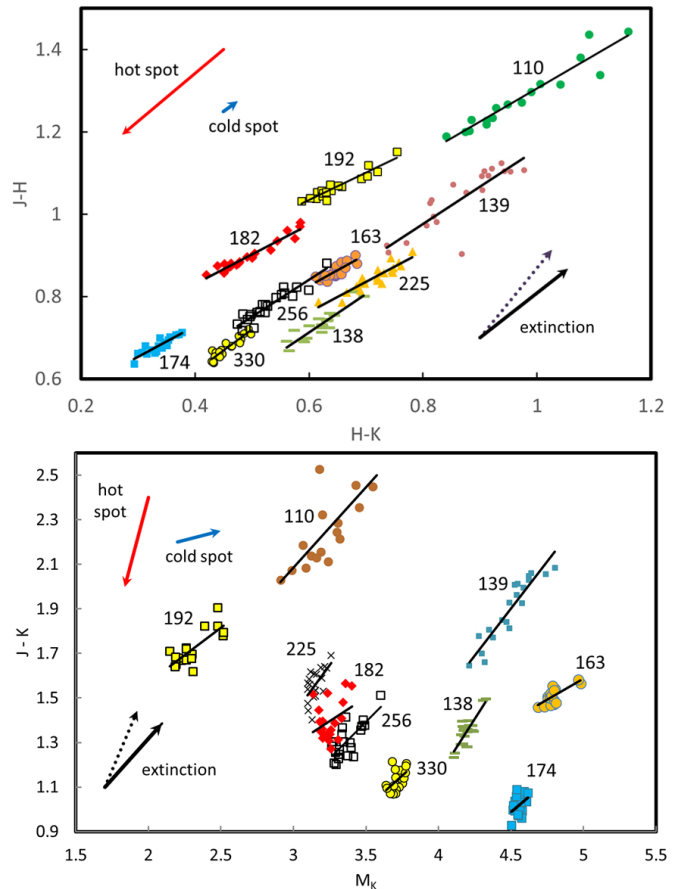


**Figure 17.** This diagram shows eleven sources where the pattern of change is consistent with variations in the amount of extinction, e.g. from inhomogeneities in a circumstellar disk. The standard interstellar extinction behavior (Rieke & Lebofsky 1985) for  $A_V = 2$  is shown as a dotted black line, and the extinction for a particle size distribution extending upward to  $\sim 1 \mu\text{m}$  (Steenman & Thé 1989) is shown as a solid black line. The behavior of a source acquiring a hot or cold spot is shown at the upper left with a red or blue arrow, respectively. The thin black lines show fits by linear regression to the data for each source.

possibilities for such events are Sources 95, 137, 146, 288, 304, and 347. These eight sources should be observed with a more rapid cadence to test this possibility.

These events could either be a result of the intervention of a luminous object, i.e., a companion star, or that these sources are “dippers” (Morales-Calderón et al. 2011), behavior characterized by Rice et al. (2015) for sources in Orion and attributed by them to the intervention of a compact dust cloud. We can distinguish the two possibilities on a general basis: dippers would usually have a stronger event the shorter the wavelength, whereas stellar eclipses would have a similar number of events with stronger or weaker events with shorter wavelength (depending on whether the hotter or the cooler member of the pair was diminished). Of the eight candidate objects, five have events at equal strength in all three bands, two (137 and 156) have stronger events the longer the wavelength, by about a factor of two from  $J$  to  $K$ , and one has a modestly stronger event at  $J$  than at  $K$  (a factor of 1.5). This distribution favors the hypothesis that they

**Table 7**  
Slopes by linear regression from Figure 17 compared with those for other extinction determinations

Source	$E(J-K)/\Delta K$	$E(H-K)/E(J-H)$
Rieke & Lebofsky (1985), $R = 3.1$	$1.50 \pm 0.2$	$1.70 \pm 0.15$
Harris et al. (1978), $\rho$ Oph $R \sim 5$		$1.40 \pm 0.15$
Cardelli et al. (1989)	1.48	1.22
He et al. (1995), general		$1.64 \pm 0.26$
He et al. (1995), $\rho$ Oph		$1.64 \pm 0.23$
Steenman & Thé (1989), $R = 5.9$	0.72	1.09
69	$0.72 \pm 0.15$	$0.81 \pm 0.07$
90	$1.01 \pm 0.17$	$0.93 \pm 0.10$
109	$0.37 \pm 0.09$	$0.77 \pm 0.13$
116	$0.57 \pm 0.31$	$0.76 \pm 0.10$
124	$0.43 \pm 0.27$	$0.72 \pm 0.05$
126	$0.50 \pm 0.09$	$0.67 \pm 0.05$
145	$0.90 \pm 0.27$	$0.74 \pm 0.07$
168	$0.66 \pm 0.14$	$0.90 \pm 0.08$
207	$0.59 \pm 0.21$	$1.00 \pm 0.10$
median	0.59	0.77

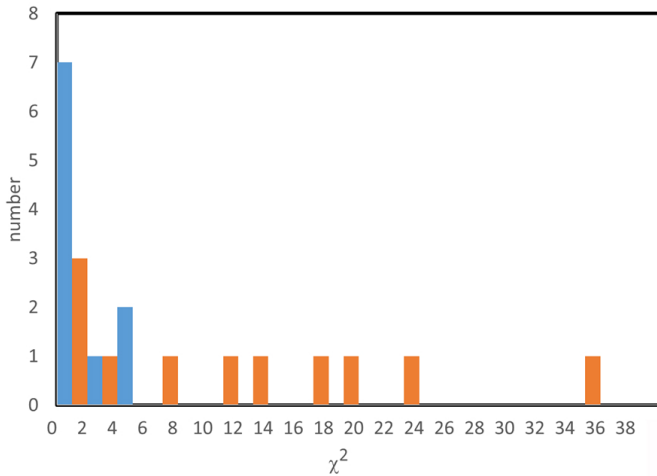


**Figure 18.** To separate sources where the variations may be dominated by extinction and those with variations dominated by accretion, we compute the reduced  $\chi^2$  relative to the relation  $(H - K) = 0.77(J - H) + \text{constant}$ . The blue bars are the sources used to study the extinction behavior (Figure 17) and the orange bars are those we suggest are dominated by accretion events (Figures 11 and 13).

are mostly due to stellar binaries, although sources 137 and 156 could also be dippers.

#### 5.6.5. Intrinsic $K$ -band variability and instabilities in circumstellar disk rims

Another class of source has the larger variations in the  $K$  band, with decreasing amplitudes for  $H$  and then  $J$ , which we will show is indicative of grains being exposed to direct stellar irradiation after being lifted out of an optically thick circumstellar disk. Two examples are shown in Figure 20. The placement of these sources on the  $H - K$ ,  $J - H$  diagram is shown in Figure 21; they tend to fall below the CTTS locus but parallel to it and in a position that is consistent with their having greater excesses in  $K$  above the photospheric emission (to the right of the stellar locus) and/or reduced hot-spot type

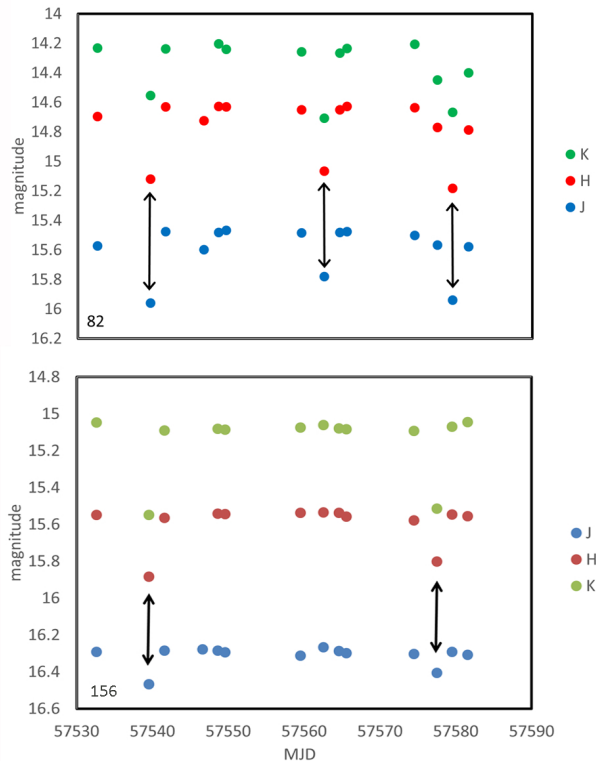


**Figure 19.** Examples of light curves suggestive of eclipses. The  $K_S$  photometry is in green,  $H$  in red, and  $J$  in blue, and the arrows indicate possible eclipses.

activity (down relative to the CTTS locus)<sup>15</sup>.

Mid-infrared variations in young stars can arise purely from instabilities in the circumstellar disk (e.g., Muzerolle et al. 2009; Flaherty et al. 2016). We will test whether such instabilities can account for the variability in our sample where the  $K$ -band changes are larger than those at  $J$  and  $H$ . The near infrared emission should originate from dust at the inner disk rim, a position regulated by the grain sublimation temperature, as is confirmed by near infrared interferometry and reverberation

<sup>15</sup> It is not uncommon for stars to be distributed around the CTTS locus rather than all being above it (e.g., Hillenbrand et al. 1998).



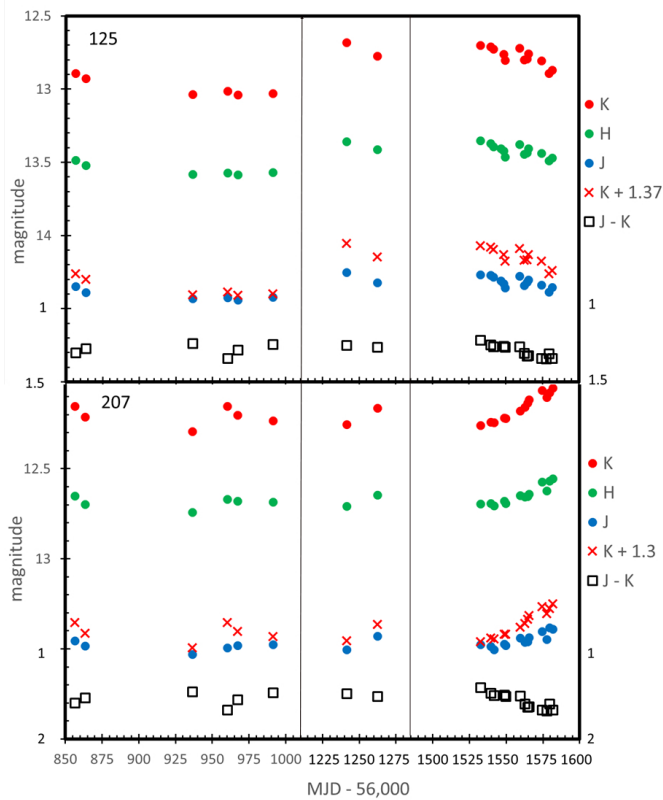


**Figure 20.** Example sources with large intrinsic variability at  $K$ , reducing toward shorter wavelengths. The  $K$  photometry is repeated fainter as indicated to facilitate comparison with that at  $J$ .

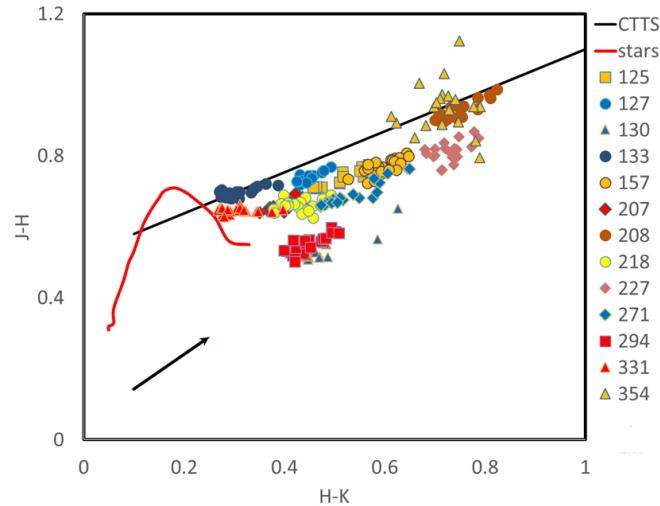


**Figure 21.** Placement of predominantly  $K$  variables on the  $H - K$ ,  $J - H$  diagram. The stellar color locus (red line) is from Luhman et al. (2010), supplemented by standard colors for types earlier than K4; the black solid line indicates the CTTS locus from Meyer et al. (1997) and the black vector shows the effect of extinction by large grains.

mapping (e.g., Millan-Gabet et al. 2007; Dullemond & Monnier 2010; Anthonioz et al. 2015; Meng et al. 2016). The  $JHK$  colors of CTTS also often show an excess attributed to emission by the inner disk (e.g., Cieza et al. 2005). The sublimation temperature is conventionally placed at 1500K, appropriate for small silicate

grains. However, the process is complex, depending on (1) grain composition; (2) ambient gas density; and (3) size and time of exposure. Specifically, the carbonaceous grain components sublimate at  $\sim 2000$ K. In addition, when silicates break down some of the products, e.g., FeO and MgO, have similarly high sublimation temperatures (Mann et al. 2007). As shown in detail by Baskin & Laor (2018), the sublimation process is one of erosion and hence the sublimation temperature is increased for grains immersed in relatively dense gas. As they also show, it takes longer to eliminate large grains, allowing transient events involving large grains (see their Section 4.6.1) to exhibit higher temperatures than for steady-state conditions with small ones.

Cieza et al. (2005); McClure et al. (2013) show that the near infrared excesses of CTTSs can be fitted with blackbodies of temperature  $1750 \pm 250$ K. For comparison, we have fitted blackbodies to the *variable* emission of the dominant  $K$ -band-variability sources, as listed in Table 8. To obtain measurements of the variable component of the emission we subtracted the measurements in a low state from those in a high one. Specifically, we took the differences in brightness on the indicated dates (averages over a range of dates if so indicated in the table) and corrected for the extinction of Tr 37 ( $A_V = 1.3$ , Rieke & Lebofsky (1985) extinction law). The fits were done by  $\chi^2$  minimization assuming a net error in the differences of 5% (including the non-statistical contribution estimated by Rice et al. (2015)) and the indicated errors in the temperatures are  $\sim \pm 200$ K. It is the nature of the fits to have the same offsets relative to the  $J$  and  $K$  measurements, they can be considered to give the  $J$  to  $K$  color temperature with an additional check that the  $H$  point is consistent. With the exception only of Source 331, satisfactory fits were achieved, that is deviations of  $\lesssim 10\%$  from the fit for the individual bands, up to  $< 20\%$  in two cases. All but one case indicates a temperature in the range appropriate for transiently heated dust from the circumstellar disk. The exception (Source 130) is for the only source where we differenced data over an interval of about a year; the other cases are all for intervals of order a month, i.e., for transient events with that timescale.

With the exception of Source 331 (where the fit of a single blackbody was unsatisfactory), the success of these fits and the small range of temperatures indicates that the  $K$ -band variations are *not* correlated with accretion events that create stellar hot spots, since as shown in Section 5.6.1, these events would force the fits to significantly warmer temperatures. Only sources 227 and 271, with fitted temperatures of  $\sim 2400$ K, (plus source 331) have any suggestion of such accretion events. Although we have dereddened the photometry for the average in Tr 37 of  $A_V = 1.3$  (Errmann et al. 2013), there is a range of reddening and some estimates are somewhat higher, e.g., from Sicilia-Aguilar et al. (2013)  $1.56 \pm 0.55$ . To bound the possibilities, we also computed temperatures after dereddening for  $A_V = 2.3$ . The conclusions are only slightly modified: now sources 227 and 271 are lifted out of the range where emission by sublimating dust is plausible. However, it is unlikely that source 271 is so strongly reddened, since that would make its intrinsic  $J - H$  color too blue compared with the other similar cluster members (Sicilia-Aguilar et al. 2010) assuming

**Table 8**  
Temperatures fitted to variable components

Source	MJD <sup>a</sup>	J (mag)	H (mag)	K (mag)	T (K) $A_V = 1.3$	T (K) $A_V = 2.3$
125	57533 - 57540	14.27	13.36	12.71	—	—
—	57580 - 57582	14.40	13.48	12.88	1970	2110
127	57550 - 57562	13.53	12.66	12.13	—	—
—	57574 - 57579	13.48	12.58	12.01	1840	1950
130	57241 - 57262	16.10	15.35	14.66	—	—
—	57532 - 57582	16.12	15.45	14.93	1150 <sup>b</sup>	1200 <sup>b</sup>
133	56960	14.00	13.14	12.67	—	—
—	56991	14.03	13.19	12.81	1590	1680
157	57533 - 57540	14.54	13.67	13.01	—	—
—	57565 - 57566	14.42	13.50	12.80	1850	1970
207	57533 - 57542	13.49	12.70	12.25	—	—
—	57580 - 57582	13.39	12.56	12.06	2130	2300
208	57242	14.40	13.29	12.40	—	—
—	57262	14.52	13.46	12.67	1570	1660
218	56960 - 56967	12.69	11.87	11.39	—	—
—	56991	12.57	11.74	11.16	2060	2210
227	56856	14.73	13.72	12.86	—	—
—	56863	14.40	13.435	12.58	2410	2620
271	56936	13.80	12.96	12.29	—	—
—	56967	13.57	12.70	12.03	2400	2620
294	57533 - 57542	16.00	15.30	14.77	—	—
—	57566	15.945	15.22	14.63	1840	1960
331	57533 - 57540	14.54	13.75	13.39	—	—
—	57562 - 57565	14.45	13.67	13.20	1890 <sup>c</sup>	1890 <sup>c</sup>
354	57549 - 57562	18.14	17.05	16.24	—	—
—	57566 - 57582	18.26	17.21	16.47	1750	1860

<sup>a</sup> Each source has two entries; the first one is the date or range of dates for the high state, and the second is the date or range of dates for the low state. The temperatures are fitted to the differences of the fluxes at each band in the high minus the low state.

<sup>b</sup> Time interval is  $\sim$  one year compared with  $\sim$  one month for the other sources.

<sup>c</sup> Poor temperature fit because indicated change at  $H$  is relatively low.

their reddening is average for Tr 37. That is, at least 10 and probably 11 of 13 stars with dominant  $K$ -band variations show colors consistent with the variable signal arising from dust heated transiently to its sublimation temperature.

This result is similar to that of Flaherty et al. (2014), who found no correlation between X-ray and mid-infrared variability of pre-main-sequence stars, i.e., that the mid-IR variations arise from the disk and are not related to simultaneous or nearly simultaneous accretion events. Instead, the behavior indicates a substantial level of turbulence at the inner disk rim, sufficient to expose otherwise protected dust to the radiation of the star. Such behavior is predicted by a number of theoretical simulations (e.g., Bans & Konigl 2012; Turner et al. 2014; Flock et al. 2017).

#### 5.6.6. Large variations of neutral color: occultation by the circumstellar disk

Surveys similar to ours but with higher cadence have shown that there are many sources that vary roughly equally in  $J$ ,  $H$ , and  $K$ , with periods of a few days to a few weeks and amplitudes of a few tenths of a magnitude. Because of the aliasing of such behavior into our lower cadence, such sources are likely to appear to have chaotic variations and we do find a significant number of such objects. Since our data are inadequate to study them in any detail, here we call attention to just one more object, source 283, with very large changes, roughly neutral in color as shown in Figure 22. The fitted temperature of

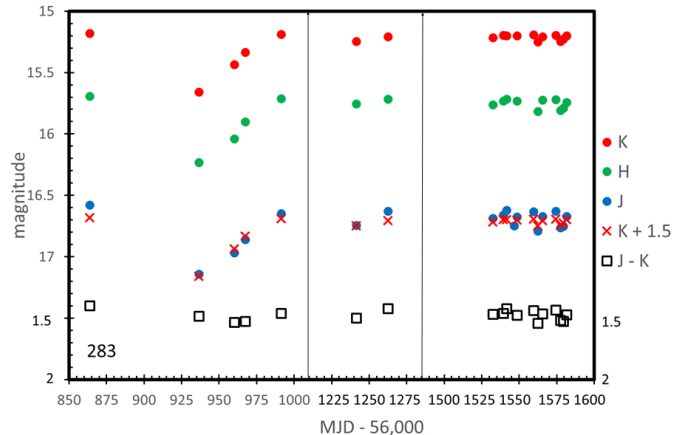


**Figure 22.** Source 283, with a large drop in all colors, otherwise with only modest variations. As shown both by the comparison of the  $K$  with the  $J$  lightcurve and the  $J - K$  color, the changes in this source are neutral in color. This object falls on the CTTS locus at a modest level to the right of the colors of normal young stars.

the change between the low state on MJD 56,936 to the high state in the last year of monitoring is 2600K, too warm to be thermal emission by the disk but cooler than expected for ongoing accretion. The excess resembles the broad and featureless continua of a sample of T Tau stars studied by Fischer et al. (2011), which they found could be fitted by blackbody spectra with temperatures between 2200 and 5000K; but see also McClure et al. (2013) who did not find this component to be necessarily present.

The  $J - H$  color of source 283 averages 0.93 and re-

mains within the errors at this value throughout its change in flux. This color is similar to the average for faint members of Tr 37 from Sicilia-Aguilar et al. (2010),  $0.87 \pm 0.10$ . The net change of 0.45 mag would require a change in the radiating area by a factor of  $\sim 1.5$ , outside the usual hot spot paradigm. Instead, the behavior resembles that of “faders” in which a warp or disruption in the circumstellar disk at a significant distance from the star creates a long-duration occultation (e.g., Hamilton et al. 2001; Bouvier et al. 2013). One example around GI Tau has a similar duration and recovery behavior to that in source 183 (Guo et al. 2018). Faders can have peculiar and relatively flat extinction variations with color (e.g., Rodriguez et al. 2016). However, the truly neutral color of the source 183 event makes it unique and might indicate that the occultation involves an optically thick disk.

## 6. VARIABLE BACKGROUND STARS

The majority of the variable stars we discovered ( $170/289 = 59\%$ ) are in the region of the CMD that indicates they are background to the Tr37 cluster. In general, these stars appear in deep optical images (e.g., Gaia), but have not been identified as having outstanding peculiarities. There is a slight shift to stars with similar amplitudes in  $J$  and  $K$  (from 54% of the cluster members to 61% of the background stars) and away from those with larger amplitudes at  $J$  (from 26% of the cluster members to 18% of the background stars); only 5 (2%) have amplitudes at  $J$  more than twice those at  $K$ , and 3 of these are sufficiently faint that the amplitudes may have relatively large errors. This low rate of strong  $J$  variability suggests a much lower fraction of strongly accreting systems in the background, as expected. Sources 175, 204, and 302 are listed by Ermann et al. (2013) as possible members of Tr 37. The first two have missing  $I$  magnitudes, presumably because they are very red, which would account for why our CMD selection would have missed them. Source 302 falls on the CMD well below the Tr37 locus, calling its membership into question.

Some of the background variables could be, for example, distant asymptotic giant branch stars. A few have interesting patterns of variability, however. We call attention to Source 69: RA = 323.521451, DEC = 57.213179 with large slow variations, Source 191: RA = 324.232413, DEC = 57.877623 which faded by a magnitude over the course of our observations, and Source 302: RA = 324.602574 and DEC = 57.460107 that showed such chaotic variations that it must have been changing output substantially during the sequence of our individual observation sets.

## 7. CONCLUSIONS

We report the results of a two-year monitoring of  $JHK$  - band variability in the Tr 37 cluster, using WFCAM on UKIRT and obtaining 21 epochs of observation. We select candidate cluster members from the  $K$ ,  $I-K$  CMD, with a check that their parallaxes from Gaia do not indicate they are foreground objects. The dividing line between background stars and cluster members was determined by the placement of reliable cluster members with accurate parallaxes from Gaia on the CMD. Only  $\lesssim 0.3\%$  of the field stars in our survey are variable, compared with  $65 \pm 8\%$  of cluster members, indicating that

our method does not mistakenly include a significant number of field stars in our cluster sample. Because this sample is selected purely on the basis of variability and location on the CMD, it should be homogeneous and suitable for studying the general behavior of the cluster members down to very low mass objects. We use the following methods to analyze the behavior of the cluster members:

- The path of the variations on the  $J-H$ ,  $H-K$  and  $J-K$ ,  $M_K$  diagrams is used to identify stars with accretion hot spots and those with variations due to extinction by dust clumps in circumstellar disks.
- Hotspots show little variation in  $K$  compared with larger variations in  $J-K$ , whereas extinction variations follow tracks of similar slope in both diagrams.
- The scatter around the color-color tracks is significantly larger for stars with accretion hotspots than for those with variable extinction.

We reach the following conclusions about the cluster members:

- Using variability to identify faint members of Tr 37, we constructed a  $K$ -band luminosity function for  $2 < M_K < 7.5$ . It drops dramatically going from the stellar range to the brown dwarf one at  $M_K \sim 6.5$ . Similar behavior has previously been observed for IC 348, a cluster of similar age. However, the luminosity function for Tr37 is shifted toward brighter absolute magnitudes (by 0.3 – 0.5 mag), suggesting that its K and M stars are somewhat younger than those in IC 348.
- The largest variations occur in the  $J$  band where a number of sources have amplitudes of  $\sim$  a factor of three. Such variations are indicative of accretion events.
- Eight sources have sharp, short drops in brightness suggestive of eclipses. These sources should be observed with a more rapid cadence than we used to test this possibility.
- Four extremely variable sources lie at the extreme for classical T Tauri star behavior and occasionally cross into having characteristics of protoplanetary disks. They may resemble EXor variables.
- Eleven sources have variability behavior consistent with varying extinction in their circumstellar disks, characterized by maximum grain sizes substantially larger than those in the general interstellar medium.
- The sources with larger variability at  $K$  than at  $J$  and  $H$  show very similar color temperatures for their variable components, close to the expected temperature for sublimation of transiently exposed dust grains. This behavior is evidence for turbulence at the inner rim of their circumstellar disks, which exposes previously shielded grains to the radiation from the star.

- One source has a long-duration dip of 0.45 mag with neutral  $JHK$  color, probably due to occultation by a warp or disturbance in a possibly optically thick circumstellar disk.

#### ACKNOWLEDGEMENTS

We thank Watson Varricatt at UKIRT for helping us with the WFCAM observations. We thank Michael A. Read (WSA, IfA, Edinburgh), for careful data reduction, image processing, and providing us the WFCAM data catalogs. We also thank Scott Wolk as referee for a critical reading of the paper. We used the UKIRT Wide Field Camera (WFCAM; Casali et al. 2007) and a photometric system described in Hewett et al. (2006). The pipeline processing and science archive are described in Irwin et al. (2007) and Hambly et al. (2008). We thank Roc Cutri for investigating the issues of deblending in the WISE data and alerting us to the likelihood of bad photometry for sources that are nominally reasonably well resolved but still close to each other on the sky. This publication makes use of data products from the Two Micron All Sky Survey, which is a joint project of the University of Massachusetts and the Infrared Processing and Analysis Center/California Institute of Technology, funded by the National Aeronautics and Space Administration and the National Science Foundation. This publication makes use of data products from the Wide-field Infrared Survey Explorer, which is a joint project of the University of California, Los Angeles, and the Jet Propulsion Laboratory/California Institute of Technology, funded by the

National Aeronautics and Space Administration. When (some of) the data reported here were acquired, UKIRT was supported by NASA and operated under an agreement among the University of Hawaii, the University of Arizona, and Lockheed Martin Advanced Technology Center; operations were enabled through the cooperation of the East Asian Observatory. The Pan-STARRS1 Surveys (PS1) and the PS1 public science archive have been made possible through contributions by the Institute for Astronomy, the University of Hawaii, the Pan-STARRS Project Office, the Max-Planck Society and its participating institutes, the Max Planck Institute for Astronomy, Heidelberg and the Max Planck Institute for Extraterrestrial Physics, Garching, The Johns Hopkins University, Durham University, the University of Edinburgh, the Queen's University Belfast, the Harvard-Smithsonian Center for Astrophysics, the Las Cumbres Observatory Global Telescope Network Incorporated, the National Central University of Taiwan, the Space Telescope Science Institute, the National Aeronautics and Space Administration under Grant No. NNX08AR22G issued through the Planetary Science Division of the NASA Science Mission Directorate, the National Science Foundation Grant No. AST-1238877, the University of Maryland, Eotvos Lorand University (ELTE), the Los Alamos National Laboratory, and the Gordon and Betty Moore Foundation.

UKIRT (WFCAM)

#### APPENDIX

In addition to the UKIRT/WFCAM data obtained for this project, we make use of the Pan-STARRS optical photometry, similar photometry by Barentsen et al. (2011), 2MASS, and WISE. This appendix discusses the methods used to adapt these data sources to our study.

#### CONVERSION OF PAN-STARRS PHOTOMETRY TO $I_{CFH12K}$

We have derived  $I$  magnitudes by reference to the  $I_{CFH12K}$  band, with an effective wavelength of 8090 Å<sup>16</sup>. We derive these magnitudes by transformation from Pan-STARRS, defined from the photometry in IC 348 by Luhman et al. (2016). Pan-STARRS uses *grizy* bands for photometry in AB magnitudes, while the photometry in Luhman et al. (2016) was based on different optical filters in Vega magnitudes. To reconcile the bandpass differences, we use the coordinates and  $I$  band magnitudes of IC 348 members with no infrared excesses<sup>17</sup> (Luhman et al. 2016) to cross-match with the Pan-STARRS DR1 astrometry and photometry (with the subscript indicating the instrument, hereafter) The  $I_{CFH12K}$  band is between those of Pan-STARRS  $i_{P1}$  and  $z_{P1}$  bands (7520 and 8660 Å, respectively, Tonry et al. 2012). Therefore, we use the  $i_{P1}$  and  $z_{P1}$  photometry of IC 348 to derive the following transformation equation,

$$I_{CFH12K} = 1.0291z_{P1} + 0.2469(i_{P1} - z_{P1}) - 0.5894 \quad (\text{A1})$$

The difference between Vega and AB magnitude systems is not a problem here as the transformation equation should have accounted for the zero point fluxes. The errors in photometric transformations are difficult to estimate; we estimate errors of 0.1 to 0.15 magnitudes for the  $I_{CFH12K}$  magnitudes. To obtain the equivalent magnitudes of the UKIRT-detected stars in the TR 37 region, we apply equation (A1) to Pan-STARRS  $i_{P1}$  and  $z_{P1}$  photometry for  $I_{CFH12K}$  and use the transformation equation from UKIRT/WFCAM to 2MASS for the  $K_{s,2MASS}$  magnitudes (Equation 5d in Hewett et al. 2006). We adopt an average extinction of  $A_V = 1.3$  (Errmann et al. 2013), corresponding to  $A_{K_{s,2MASS}} = 0.148$  and  $E(I_{CFH12K} - K_{s,2MASS}) = 0.491$  assuming the extinction law with  $R_V = 3.1$ , to correct the interstellar extinction of all stars detected by UKIRT.

#### IDENTIFICATION OF VARIATIONS BETWEEN 2MASS AND 2MASS 6X MEASUREMENTS

We computed the significance (in standard deviations) of the changes between the 2MASS and 2MASS 6X measurements in each band,  $J$ ,  $H$ , and  $K$ , and using the tabulated error estimates. A source was identified as being variable

<sup>16</sup> <http://www.cfht.hawaii.edu/Instruments/Filters/cfh12k.html>

<sup>17</sup> The coefficients of magnitude conversion are slightly dependent on the input spectrum. Although no significant excess is expected at visible wavelengths, to be conservative we only use IC 348 member stars without infrared excesses to derive the transformation equation.

if it varied by at least  $2\sigma$  and in the same direction in at least two bands. This approach is roughly equivalent to requiring a Stetson Index  $\gtrsim 1$ , although with only two observations this parameter is probably not fully appropriate.

#### IDENTIFICATION OF VARIABILITY IN WISE DATA

An issue with WISE is source confusion and unreliable deblending of close sources (Roc Cutri, private communication). We inspected the image of each source and flag as “conf.” those that appeared blended. We also found that a moderately brighter source within  $15''$  could affect the photometry, as could a source of comparable brightness within  $10''$ . Both cases are also marked “conf.”, as are any cases with sources within one beam width ( $6''5$ ) and bright enough to affect the results. All such sources were rejected from the further analysis.

Nominally, with a total of  $\sim 50$  measurements in each of the two relevant WISE bands, having a  $2\sigma$  fluctuation in the same direction in both bands would already indicate a real variation with reasonable confidence. However, this is not a very conservative threshold, particularly if there is a possibility, e.g., that non-statistical fluctuations are correlated between the bands (such behavior could also “fool” the Stetson Index). Given the large number of measurements, we could base the identification of variables on the scatter within the data. We computed an overall mean and standard deviation for all the measurements of a source in a given band. We then set a flag if in the same measurement set (i.e., at the same time) there was a deviation from this mean by  $\geq 2\sigma$  in both bands. However, given the number of such cases, we need to calibrate the significance level associated with the nominal standard deviation. We found that the number of these flags for a given source dropped quickly from many cases with a single flag to a much lower incidence of five flags, and then persisted at similar levels to much larger numbers of flags, indicating that six and more flags were finding true variations, whereas fewer flags were contaminated by noise. We therefore identified a source as variable if it had 6 or more of these flags, i.e., it exceeded  $2\sigma$  from the mean in both bands in at least six measurement pairs. We identified the variations as fast if they were apparent in one or two of the 2-3 day series and slow if they appeared as a shift between the series.

## REFERENCES

- Anthonioz, F., Ménard, F., Pinte, C., et al. 2015, *A&A*, 574, 41  
 Audard, M., Ábrahám, O., Dunham, M. M. et al. 2014, in *Protostars and Planets VI*, ed. Beuther, Klessen, Dullemond, & Henning, University of AZ Press: Tucson, AZ, pp 387 - 410  
 Bans, A., & Kónigl, A. 2012, *ApJ*, 758, 100  
 Barentsen, G., Vink, J. S., Drew, J. E. 2011, *MNRAS*, 415, 103  
 Barentsen, G., Farnhill, H. J., Drew, J. E. et al. 2014, *MNRAS*, 444, 3230  
 Baskin, A., & Laor, A. 2018, *MNRAS*, 474, 1970  
 Bouvier, J., Grankin, K., Ellerbroek, L. E., Bouy, H., & Barrado, D. 2013, *A&A*, 557, A77  
 Boyce, Madeline, Ruiz-Rodriguez, Dary, & Kastner, Joel 2019, 233rd AAS meeting poster  
 Budavári, T., Szalay, A. S. & Fekete, G. 2010, *PASP*, 122, 1375  
 Cardelli, J. A., Clayton, G. C., & Mathis, J. S. 1989, *ApJ*, 645, 245  
 Carpenter, J. M., Hillenbrand, L. A., & Skrutskie, M. F. 2001, *AJ*, 121, 3160  
 Casali, M., Adamson, A., Alves de Oliveira, C. et al. 2007, *A&A*, 467, 777  
 Chambers, K. C., Magnier, E. A., Metcalfe, N. et al. 2016, arXiv:1612.05560  
 Cieza, L. A., Kessler-Silacci, J. E., Jaffe, D. T., Harvey, P. M., & Evans, N. J. 2005, *ApJ*, 635, 422  
 Contreras, M. E., Sicilia-Aguilar, A., Muzerolle, J., Calvet, N., Berlind, P., & Hartmann, L. 2002, *AJ*, 124, 1585  
 Cross, N. J. G., Collins, R. S., Hambly, N. C. 2009, *MNRAS*, 399, 1730  
 Cutri, R. M., Skrutskie, M. F., van Duk, S. et al. 2003, "The IRSA 2MASS All-Sky Point Source Catalog, NASA/IPAC Infrared Science Archive."  
<http://irsa.ipac.caltech.edu/applications/Gator/>  
 Cutri, R. M., Skrutskie, M. F., van Dyk, S. et al. 2012, *VizieR Online Data Catalog: 2MASS 6X Point Source Working Database*  
 De Oliveira, A. & Casali, M. 2008, *A&A*, 485, 155  
 Dullemond, C. P., & Monnier, J. D. 2010, *ARA&A*, 48, 205  
 Errmann, R., Neuhäuser, R., Marschall, L. et al. 2013, *Astronomische Nachrichten*, 334, 673  
 Fischer, W., Edwards, S., Hillenbrand, L., & Kwan, J 2011, *ApJ*, 730, 73  
 Flaherty, K. M., Muzerolle, J., Wolk, S. J. et al. 2014, *ApJ*, 793, 2  
 Flaherty, K. M., DeMarchi, L., Muzerolle, J. et al. 2016, *ApJ*, 833, 104  
 Flock, M., Fromang, S., Turner, N. J., & Benisty, M. 2017, *ApJ*, 835, 230  
 Gaia Collaboration 2018, *A&A*, 616A, 1  
 Getman, K. V., Feigelson, E. D., Sicilia-Aguilar, A. et al. 2012, *MNRAS*, 426, 2917  
 Giannini, T., Lorenzetti, D., Antonucci, S. et al. 2016, *ApJL*, 819, 5  
 Giannini, T., Antonucci, S., Lorenzetti, D. et al. 2017, *ApJ*, 839, 112  
 Günther, H. M., Cody, A. M., Covey, K. R. et al. 2014, *AJ*, 148, 122  
 Guo, Z., Herczeg, G. J., Jose, J. et al. 2018, *ApJ*, 852, 56  
 Guitermuth, R. A., Megeath, S. T., Myers, P. C. et al. 2009, *ApJS*, 184, 18  
 Hambly, N. C., Collins, R. S., Cross, N. J. G. et al. 2008, *MNRAS*, 384, 637  
 Hamilton, C. M., Herbst, W., Shih, C., & Ferro, A. J. 2001, *ApJL*, 554, 201  
 Harris, D. H., Woolf, N. J., & Rieke, G. H. 1978, *ApJ*, 226, 829  
 He, L., Whittet, D. C. B., Kilkenny, D., & Spencer Jones, J. H. 1995, *ApJS*, 101, 335  
 Herbst, W. 2008, in *Handbook of Star Forming Regions: Volume I, The Northern Sky*, ASP Monograph Publications, Vol. 4, ed. B. Reipurth (San Francisco, CA: ASP), 372  
 Hewett, P. C., Warren, S. J., Leggett, S. K. & Hodgkin, S. T. 2006, *MNRAS*, 367, 454  
 Hillenbrand, L. A., Strom, S. E., Calvet, N. et al. 1998, *AJ*, 116, 1816  
 Hodgkin, S. T., Irwin, M. J., Hewett, P. C. & Warren, S. J. 2009, *MNRAS*, 394, 675  
 Irwin, M. J., Lewis, J., Hodgkin, S. et al. 2004, *SPIE*, 5493, 411  
 Irwin, J., Irwin, M., Aigrain, S. et al. 2007, *MNRAS*, 375, 1449  
 Luhman, K. L., Stauffer, J. R., Muench, A. A. et al. 2003, *ApJ*, 593, 1093  
 Luhman, K. L., Allen, P. R., Espaillat, C., Hartmann, L., & Calvet, N. 2010, *ApJS*, 186, 111  
 Luhman, K. L., Esplin, T. L. & Loutrel, N. P. 2016, *ApJ*, 827, 52  
 Mann, Ingrid, Murad, Edmons, & Czechowski, Andrzej 2007, *Plan. & Sp. Sci.*, 55, 1000  
 Marschall, L. A., & van Altena, W. F. 1987, *AJ*, 94, 71  
 McClure, M. K., Calvet, N., Espaillat, C., et al. 2013, *ApJ*, 769, 73  
 Megeath, S. T., Gutermuth, R., Muzerolle, J. et al. 2012, *AJ*, 144, 192  
 Meng, H. Y. A., Plavchan, P., Rieke, G. H. et al. 2016, *ApJ*, 823, 58  
 Meng, H. Y. A., Rieke, G. H., Su, K. Y. L., & Gáspár, A. 2017, *ApJ*, 836, 34  
 Meyer, M. R., Calvet, Nuria, & Hillenbrand, L. A. 1997, *AJ*, 114, 288  
 Millan-Gabet, R., Malbet, F., Akeson, R., et al. 2007, in *Protostars and Planets V*, ed. B. Reipurth, D. Jewitt, & K. Keil (Tucson, AZ: Univ. Arizona Press), 539  
 Morales-Calderón, M., Stauffer, J. R., Rebull, L. et al. 2009, *ApJ*, 702, 1507  
 Morales-Calderón, M., Stauffer, J. R., Hillenbrand, L. A. et al. 2011, *ApJ*, 733, 50  
 Muench, A. A., Lada, E. A., Lada, C. J. et al. 2003, *AJ*, 125, 2029  
 Muzerolle, J., Flaherty, K., Balog, Z. et al. 2009, *ApJL*, 704, 15  
 Nakano, M., Sugitani, K., Watanabe, M. et al. 2012, *AJ*, 143, 61  
 Parks, J. R., Plavchan, P., White, R. J., & Gee, A. H. 2014, *ApJS*, 211, 3  
 Pietrukiwicz, P., Minniti, D., Fernández, J. M. et al. 2009, *A&A*, 503, 651  
 Platais, Imants, Kozhurina-Platais, Vera, & van Leeuwen, Floor 1998, *AJ*, 116, 2423  
 Poppenhaeger, K., Cody, A. M., Covey, K. R. et al. 2015, *AJ*, 150, 118  
 Rebull, L. M., Cody, A. M., Covey, K. R. et al. 2014, *AJ*, 148, 92  
 Rebull, L. M., Stauffer, J. R., Cody, A. M. et al. 2015, *AJ*, 150, 175  
 Ribas, A., Bouy, H., & Merín, B. 2015, *A&A*, 576A, 52  
 Rice, T. S., Wolk, S. J., & Aspin, C. 2012, *ApJ*, 755, 65  
 Rice, T. S., Reipurth, Bo, Wolk, S. J., Vaz, L. P., & Cross, N. J. G. 2015, *MNRAS*, 150, 132  
 Rieke, G. H., & Lebofsky, M. J. 1985, *ApJ*, 288, 618  
 Rodriguez, J. E., Reed, P. A., Siverd, R. J. et al. 2016, *AJ*, 151, 29  
 Scholz, A., Froebrich, D., Davis, C. J., & Meusinger, H. 2010, *MNRAS*, 406, 505  
 Sesar, B., Ivezić, Ž., Lupton, R. H. et al. 2006, *AJ*, 134, 2236  
 Sicilia-Aguilar, A., Hartmann, L. W., Briceño, C., Muzerolle, J. & Calvet, N. 2004, *AJ*, 128, 805  
 Sicilia-Aguilar, A., Hartmann, L. W., Hernández, J., Briceño, C. & Calvet, N. 2005, *AJ*, 130, 188  
 Sicilia-Aguilar, A., Hartmann, L., Calvet, N. et al. 2006, *ApJ*, 638, 897  
 Sicilia-Aguilar, A., Hartmann, L. W., Fűrész, G. et al. 2006b, *AJ*, 132, 2135  
 Sicilia-Aguilar, A., Henning, T., & Hartmann, L. W. 2010, *ApJ*, 710, 597  
 Sicilia-Aguilar, A., Kim, J. S., Sobolev, A. et al. 2013, *A&A*, 559, 3  
 Sicilia-Aguilar, A., Roccatagliata, V., Getman, K. et al. 2015a, *A&A*, 573, A19  
 Sicilia-Aguilar, A., Patel, N., Fang, M., et al. 2019, *A&A*, 622A, 118  
 Skrutskie, M. F., Cutri, R. M., Stiening, R. et al. 2006, *AJ*, 131, 1163  
 Stetson, P. B. 1996, *PASP*, 108, 851  
 Stauffer, J., Cody A. M., McGinnis, P. et al. 2015, *AJ*, 149, 130  
 Steenman, H., & Thé, P. S. 1989, *Ap&SS*, 159, 189  
 Steenman, H., & Thé, P. S. 1989, *Ap&SS*, 184, 9  
 Stetson, P. B. 1996, *PASP*, 108, 851  
 Strateva, I., Ivezić, Ž., Knapp, G. R. et al. 2001, *AJ*, 122, 1861  
 Tonry, J. L., Stubbs, C. W., Lykke, K. R. et al. 2012, *ApJ*, 750, 99  
 Turner, N. J., Benisty, M., Dullemond, C. P., & Hirose, S. 2014, *ApJ*, 780, 42  
 Werner, M. K., Roellig, T. L., Low, F. J. et al. 2004, *ApJS*, 154, 1

Wolk, S. J., Rice, T. S., & Aspin, C. 2013a, ApJ, 773, 145

Wolk, S. J., Rice, T. S., & Aspin, C. 2013b, AJ, 145, 113

Wolk, S. J., Günther, H. M., Poppenhaeger, K. et al. 2018, AJ,  
155, 99

Wright, E. L., Eisenhardt, P. R. M., Mainzer, A. K. et al. 2010,  
AJ, 140, 1868

Xu, Shuangjing, Zhang, Bo, Reid, M. J., Zheng, Xingwu, & Wanf,  
Guangli 2019, arXiv 1903.04105v2





Table 3 — *Continued*

ID	RA	DEC	$I$	$J$	$H$	$K$	$\Delta J$	$\Delta H$	$\Delta K$	$\langle S \rangle$	var type <sup>a</sup>	Previous ID <sup>b</sup>	FX ( $10^{-6}$ ph cm $^{-2}$ s $^{-1}$ )
243	324.355784	58.047985	19.19	16.39	15.17	14.07	1.14	0.82	0.70	7.22	c, EXOR <sup>e</sup>		
247	324.366043	57.367966	17.97	15.44	14.80	14.31	0.14	0.15	0.17	1.67	b	/SA13	
250	324.370581	57.601202	15.92	13.96	13.08	12.59	0.22	0.22	0.19	1.74	b	1476/14-1017	
251	324.375083	57.502818	19.35	16.71	15.69	15.00	0.49	0.44	0.30	3.44	c, fader		
252	324.377699	57.583802	16.75	14.67	13.82	13.34	0.52	0.50	0.46	5.28	b,ext <sup>e</sup>		1.20
256	324.392136	57.575332	17.52	14.79	13.86	13.24	0.67	0.51	0.35	4.77	c, ext <sup>e</sup>	/SA13	
257	324.394358	57.2827	16.66	14.75	13.89	13.33	0.25	0.22	0.24	2.04	b		
260	324.404686	57.553127	18.66	15.96	15.25	14.65	0.20	0.15	0.15	1.56	c		
262	324.411844	57.493595	15.06	13.28	12.43	11.86	0.34	0.23	0.30	1.68	b		5.70
270	324.432851	57.581181	17.73	15.31	14.61	14.11	0.16	0.16	0.12	1.15	c	/SA13	
271	324.438118	57.328395	15.42	13.76	12.94	12.32	0.26	0.33	0.44	2.71	a	1425/11-383 <sup>d</sup>	
272	324.452311	57.405119	20.22	17.41	16.15	15.06	1.15	1.14	0.98	8.15	a, EXOR <sup>e</sup>		
273	324.453945	57.389145	16.40	15.11	14.02	13.29	1.11	0.71	0.41	8.05	c, hs <sup>e</sup>	1803/SA13	
275	324.459157	57.561204	14.92	13.19	12.44	12.16	0.25	0.26	0.22	3.24	b	1475/13-924	12.00
276	324.459286	57.430197	14.86	13.20	12.52	12.24	0.17	0.15	0.13	1.87	c	1442/12-1984	
278	324.463395	57.410042	17.65	15.43	14.71	14.18	0.19	0.24	0.24	2.04	b	/SA13	
280	324.468527	57.312628	19.48	16.70	15.93	15.32	0.44	0.42	0.34	4.10	b, EXOR		
283	324.472888	57.82341	19.26	16.69	15.77	15.23	0.54	0.54	0.48	3.62	b, fader <sup>e</sup>		
288	324.490098	57.379908	14.70	12.96	12.15	11.65	0.40	0.32	0.36	2.45	b, eclipse	1432/12-1091	
289	324.492206	57.522185	14.64	12.75	12.02	11.72	0.17	0.15	0.17	1.91	b	1468/13-269	9.20
291	324.494683	57.467932	19.04	16.26	15.60	15.00	0.15	0.16	0.13	1.53	b		
292	324.508504	57.675229	19.15	16.20	15.64	15.14	0.13	0.16	0.10	1.37	b		
293	324.511704	57.524318	19.27	16.57	15.86	15.28	0.40	0.30	0.20	3.06	c		
294	324.516183	57.494062	18.33	16.00	15.30	14.76	0.08	0.19	0.25	1.21	a, dsk <sup>e</sup>		
295	324.524786	57.378836	15.96	14.24	13.48	13.23	0.15	0.14	0.13	1.49	b	1431/12-1081	
304	324.550068	57.41689	16.30	14.48	13.68	13.30	0.47	0.44	0.44	1.65	b, eclipse, hs <sup>e</sup>	/SA13	
305	324.550552	57.748448	16.65	14.92	14.16	13.87	0.11	0.13	0.10	1.12	b		
307	324.567262	57.326586	15.82	13.96	13.19	12.82	0.18	0.16	0.18	1.23	b	1548/54-1781 <sup>d</sup>	
316	324.592222	58.014535	17.67	15.28	14.26	13.79	0.18	0.19	0.17	2.40	b		
317	324.599777	57.460071	16.76	14.83	14.04	13.64	0.13	0.12	0.10	0.89	b	/SA13	
320	324.608193	57.569264	14.69	13.01	12.32	12.04	0.21	0.20	0.19	3.19	b	1473/13-819	
324	324.616835	57.793438	17.45	15.40	14.67	14.25	0.19	0.17	0.10	1.23	c	/SA13	
327	324.618354	58.009658	16.75	14.82	13.99	13.69	0.10	0.11	0.10	1.27	b		
329	324.62345	57.952692	16.48	14.66	13.82	13.53	0.06	0.09	0.07	0.92	b		
330	324.626305	57.54866	17.02	14.94	14.13	13.60	0.24	0.19	0.14	2.19	c, ext <sup>e</sup>	/SA13	
331	324.626473	57.438407	16.36	14.50	13.70	13.33	0.10	0.09	0.22	1.18	a, dsk <sup>e</sup>	/SA13	
332	324.631074	57.483683	16.36	14.49	13.68	13.37	0.11	0.13	0.15	1.10	a		
333	324.643525	57.984008	17.33	15.04	14.19	13.78	0.28	0.29	0.31	3.15	b		
338	324.668243	57.643723	14.95	13.45	12.73	12.51	0.17	0.20	0.16	1.51	b	1461/13-1709	
340	324.680512	57.309982	14.85	13.38	12.68	12.48	0.09	0.08	0.11	0.96	b	1547/54-1613	
341	324.681252	57.45753	16.35	14.15	13.45	13.05	0.13	0.14	0.12	0.91	b	1591/	
342	324.682124	57.517568	16.51	14.62	13.82	13.51	0.21	0.17	0.17	1.52	b	1821/	
347	324.709077	57.345576	18.71	16.53	15.59	14.84	0.26	0.21	0.17	1.59	c, eclipse		
348	324.710026	57.501415	14.86	13.22	12.52	12.30	0.16	0.14	0.17	1.77	b	1823/	
350	324.713426	57.62376	16.82	14.82	14.09	13.79	0.11	0.15	0.15	1.10	a		
354	324.726787	57.352163	20.50	18.18 <sup>c</sup>	17.11 <sup>c</sup>	16.34	0.31	0.31	0.41	1.94	a, dsk <sup>e</sup>		
355	324.727654	57.590015	17.75	15.10	14.50	14.02	0.18	0.13	0.19	1.37	b		

<sup>a</sup> a = variability is > 30% larger in magnitudes at  $K$  than at  $J$ ; b = variability is within 30% of the same in magnitudes at  $J$  and  $K$ ; c = variability is > 30% larger at  $J$  than at  $K$ . If the source is illustrated in the text as a variability type, the information is also provided. The relative sizes of the variations in  $J$  and  $K$  provide hints of the type of variations: category “a” is likely to vary through instabilities at the inner edge of the circumstellar disk resulting in different exposure of the disk dust; category “c” can arise either through extinction or accretion hot spots; in general the ratio  $\Delta J/\Delta K$  is < 2 for extinction variations and > 2 for hot spot ones.

<sup>b</sup> Previous designations are given as Errmann et al. (2013)/Sicilia-Aguilar. The latter cases are with the designation from Sicilia-Aguilar et al. (2006a) or by SA13 if the identification is in Sicilia-Aguilar et al. (2013).

<sup>c</sup> nominal error between 0.01 and 0.02 mag

<sup>d</sup> also SA13

<sup>e</sup> illustrated in text

**Table 4**  
Additional Variable Sources in the UKIRT Field

ID	<i>RA</i>	<i>DEC</i>	<i>I</i>	<i>J</i>	<i>H</i>	<i>K</i>	$\Delta J$	$\Delta H$	$\Delta K$	$\langle S \rangle$	var type <sup>a</sup>
1	323.087714	57.804996	16.79	15.26	14.84	14.62	0.46	0.42	0.43	3.81	b
2	323.092506	57.882082	17.48	15.71	15.16	14.88	0.28	0.24	0.25	2.29	b
3	323.111617	57.645629	15.31	13.99	13.58	13.38	0.08	0.07	0.07	0.95	b
4	323.112026	57.780937	16.64	15.20	14.80	14.57	0.21	0.26	0.34	1.77	a
5	323.121516	57.747625	19.15	17.40	16.72	16.44	0.30	0.14	0.18	1.15	c
6	323.125681	57.316271	19.33	17.18	16.27	15.91	0.26	0.28	0.13	1.60	c
7	323.126663	57.684533	19.44	17.46	16.79	16.46	0.30	0.21	0.25	1.32	b
8	323.134168	57.650785	16.64	15.09	14.60	14.37	0.11	0.12	0.12	1.11	b
9	323.134996	57.250959	19.03	17.20	16.46	16.16	0.37	0.35	0.31	2.56	b
10	323.138685	57.668148	19.21	17.43	16.83	16.55	0.17	0.14	0.17	1.10	b
12 <sup>b</sup>	323.14253	57.413697	20.72	19.12	18.43	18.14	0.52	0.44	0.35	1.09	c
14	323.157196	57.272897	17.77	16.18	15.75	15.46	0.13	0.11	0.14	1.14	b
17	323.163948	57.722862	18.54	17.03	16.55	16.28	0.49	0.47	0.46	3.27	b
18	323.164144	57.591026	18.09	16.62	16.19	15.92	0.19	0.17	0.19	1.49	b
19	323.170295	57.598284	19.05	17.45	16.74	16.43	0.53	0.63	0.49	2.39	b
20 <sup>b</sup>	323.176043	57.842399	20.40	18.33	17.52	17.13	0.96	0.70	0.61	1.77	c
21	323.190978	57.602207	18.44	16.41	15.56	15.25	0.08	0.08	0.13	1.13	a
22	323.195221	57.378041	17.60	16.19	15.67	15.48	0.09	0.08	0.12	1.04	b
23 <sup>b</sup>	323.199108	57.320508	20.07	18.46	17.97	17.68	0.27	0.98	0.14	3.79	c
26	323.20977	57.476688	19.99	17.97	17.22	16.85	0.59	0.60	0.69	1.80	b
27	323.210449	57.361217	19.03	17.24	16.64	16.32	0.47	0.33	0.34	4.03	c
29 <sup>b</sup>	323.228421	57.373886	20.21	18.41	17.75	17.46	0.41	0.47	0.49	1.20	b
32 <sup>b</sup>	323.258973	57.570637	20.34	18.30	17.61	17.24	0.76	0.55	0.46	0.91	c
33 <sup>b</sup>	323.260957	57.585283	20.80	18.74	17.97	17.66	0.40	0.29	0.32	1.01	b
34	323.261721	57.514945	18.17	16.00	15.31	14.98	0.39	0.34	0.36	1.50	b
35	323.262241	57.431169	17.99	16.58	16.18	15.99	0.35	0.35	0.26	1.57	c
37	323.283817	57.682841	16.19	14.69	14.18	13.94	0.29	0.30	0.40	2.46	a
38 <sup>b</sup>	323.285754	57.236461	19.91	18.27	17.69	17.49	0.23	0.19	0.30	1.01	b
39 <sup>b</sup>	323.286628	57.45166	20.19	18.23	17.52	17.24	0.17	0.25	0.50	1.85	a
40	323.287198	57.495891	18.76	16.88	16.33	15.99	0.14	0.11	0.17	1.20	b
41	323.308218	58.022747	19.66	17.83	17.13	16.87	0.59	0.45	0.57	2.05	b
42	323.315726	57.437379	19.02	17.42	16.76	16.55	0.60	0.47	0.63	1.13	b
43	323.322969	57.374909	18.35	16.53	15.84	15.54	0.54	0.49	0.45	4.77	b
44	323.337979	57.334491	18.72	17.20	16.63	16.39	0.31	0.30	0.36	2.63	b
46	323.350695	57.528141	15.15	13.76	13.37	13.12	0.08	0.06	0.10	0.93	a
47	323.358106	57.757981	19.21	17.48	16.84	16.55	0.31	0.31	0.31	1.79	b
49	323.386418	57.566478	18.87	17.04	16.30	16.00	0.30	0.35	0.29	2.60	b
50	323.386587	58.012326	18.29	16.63	16.05	15.79	0.05	0.05	0.07	1.10	a
51	323.390031	57.366738	18.24	16.24	15.42	15.07	0.17	0.14	0.14	1.67	b
52 <sup>b</sup>	323.393483	57.299969	19.93	18.09	17.38	17.12	0.55	0.45	0.44	1.20	b
53	323.403506	57.431624	17.36	15.82	15.18	14.93	0.76	0.71	0.76	6.66	b
54	323.405722	57.3854	16.08	14.50	14.02	13.77	0.12	0.10	0.08	1.31	c
55	323.409375	57.979593	19.20	17.61	17.05	16.82	0.42	0.38	0.33	1.74	b
56	323.416614	57.564088	18.13	16.39	15.79	15.50	0.16	0.15	0.16	1.70	b
57	323.426413	57.473667	21.96	19.00	17.86	17.37	0.78	0.58	0.70	1.12	b
58	323.438418	57.718723	19.59	17.74	17.08	16.75	0.50	0.38	0.58	3.49	b
59	323.46143	58.069593	17.97	16.15	15.49	15.17	0.35	0.31	0.25	1.19	c
60	323.468115	57.256949	19.49	17.23	16.61	16.23	0.48	0.36	0.55	1.36	b
61	323.473059	57.913125	17.98	16.22	15.59	15.29	0.40	0.30	0.32	2.75	b
62	323.478198	57.710372	18.99	17.31	16.74	16.48	0.20	0.26	0.54	1.21	a
63	323.479179	57.579409	18.95	17.50	17.01	16.81	0.58	1.34	1.41	5.74	a
64	323.490648	57.938277	16.81	15.19	14.74	14.49	0.50	0.43	0.49	4.69	b
65	323.492436	57.582291	19.02	17.35	16.72	16.47	0.24	0.27	0.25	1.00	b
66	323.495273	58.005547	19.61	17.87	17.27	17.00	0.51	0.72	0.40	1.23	b
67 <sup>b</sup>	323.49765	57.354247	21.85	19.11	18.28	17.53	0.65	0.63	0.56	1.26	b
68	323.49834	57.650886	18.81	16.71	16.05	15.72	0.37	0.33	0.32	1.68	b
69	323.500948	57.862445	17.82	16.00	15.38	15.12	0.15	0.14	0.16	1.04	b
70	323.514791	57.270579	17.43	16.02	15.53	15.34	0.29	0.34	0.38	1.15	a
71	323.519798	58.058252	17.26	15.59	14.98	14.74	0.31	0.29	0.31	3.11	b
72	323.52142	57.835732	19.20	17.33	16.70	16.40	0.19	0.18	0.21	1.05	b
73	323.521451	57.213179	18.08	16.60	16.05	15.79	0.71	0.71	0.74	6.14	b
74	323.524292	57.860506	18.33	16.53	15.95	15.67	0.17	0.12	0.18	1.05	b
76	323.528959	57.411418	17.63	16.16	15.74	15.47	0.17	0.17	0.17	1.19	b
77 <sup>b</sup>	323.531376	58.061735	20.61	18.65	17.81	17.53	0.58	0.74	0.51	1.20	b
80	323.540674	57.876418	16.56	14.79	14.22	13.92	0.43	0.26	0.24	3.26	c
81	323.541369	57.73884	17.31	15.84	15.36	15.13	0.47	0.43	0.42	2.78	b
83	323.554015	58.07293	19.79	17.73	16.91	16.62	0.28	0.33	0.33	1.46	b
85	323.565287	57.640771	16.90	15.29	14.85	14.58	0.11	0.07	0.10	1.00	b
86	323.56691	57.565278	19.65	17.89	17.17	16.84	0.46	0.30	0.41	1.16	b
87	323.568397	57.538836	18.07	16.35	15.91	15.68	0.65	0.60	0.60	8.09	b
88	323.57009	57.634729	19.53	17.80	17.22	16.89	0.70	0.59	0.44	2.04	c
90	323.582285	58.050798	18.16	16.67	16.16	15.94	0.15	0.16	0.08	1.04	c
92	323.585511	57.856912	16.20	14.57	14.06	13.79	0.15	0.11	0.13	0.89	b
93 <sup>b</sup>	323.586813	57.835386	20.79	18.79	18.00	17.63	0.62	0.60	0.48	1.26	c

Table 4 — *Continued*

ID	RA	DEC	I	J	H	K	$\Delta J$	$\Delta H$	$\Delta K$	$\langle S \rangle$	var type <sup>a</sup>
94 <sup>b</sup>	323.587007	57.413254	20.43	18.68	17.99	17.63	0.69	0.68	0.64	2.22	b
96	323.603163	57.401309	18.28	16.28	15.41	15.00	0.41	0.41	0.37	4.10	b
97	323.613641	57.927001	19.30	17.43	16.71	16.41	0.59	0.57	0.50	4.01	b
98 <sup>b</sup>	323.621399	57.367538	19.67	18.14	17.56	17.36	0.21	0.36	0.93	1.15	a
99	323.628147	57.728304	18.86	16.99	16.27	15.96	0.55	0.50	0.52	2.89	b
100 <sup>b</sup>	323.630312	57.322596		19.10	18.15	17.80	1.20	1.03	1.36	5.75	b
102	323.645365	57.63855	14.56	13.22	12.87	12.65	0.18	0.10	0.13	1.06	c
103 <sup>b</sup>	323.65668	57.667336	20.27	18.36	17.60	17.27	0.55	0.60	0.77	1.33	a
104	323.665334	57.848147	17.24	15.56	15.00	14.74	0.16	0.13	0.11	1.09	c
105	323.674717	57.855757	17.26	15.43	14.75	14.47	0.18	0.14	0.18	0.77	b
106 <sup>b</sup>	323.679355	57.976773	20.02	18.34	17.77	17.45	0.16	0.50	0.37	1.21	a
108	323.700662	57.79019	20.34	18.02	17.05	16.67	0.59	0.51	0.61	1.45	b
109	323.704057	57.499522	19.25	17.57	16.87	16.65	0.42	0.39	0.33	2.09	b
111	323.705577	57.865915	19.15	17.15	16.46	16.12	0.39	0.24	0.41	1.22	b
114 <sup>b</sup>	323.735538	57.967161	19.85	18.08	17.54	17.24	0.46	0.58	0.35	1.87	c
115	323.737388	58.029783	18.93	17.25	16.66	16.39	0.37	0.47	0.52	2.38	a
116	323.744668	57.807853	19.18	17.34	16.73	16.42	0.38	0.32	0.38	1.06	b
117	323.747966	57.597303	19.35	17.62	17.00	16.76	0.18	0.22	0.16	1.53	b
118	323.753595	58.078142	19.43	17.42	16.74	16.40	0.39	0.54	0.36	2.14	b
119	323.754716	57.821277	18.42	16.68	16.03	15.73	0.73	0.61	0.74	5.62	b
123	323.795449	57.561498	16.79	15.47	15.00	14.82	0.09	0.10	0.11	1.04	a
126 <sup>b</sup>	323.820933	58.027476	20.44	18.45	17.76	17.46	0.36	0.65	0.67	1.13	a
128	323.826282	57.766798	19.17	17.39	16.86	16.58	0.34	0.37	0.50	0.81	a
136 <sup>b</sup>	323.866887	57.335052	20.18	18.35	17.77	17.49	0.22	0.25	0.51	1.70	a
141	323.882842	57.63899	18.07	16.45	15.89	15.67	0.12	0.13	0.24	1.00	a
143	323.895524	57.428884	18.51	16.51	15.76	15.41	0.23	0.23	0.25	2.27	b
144 <sup>b</sup>	323.900029	57.644818	20.01	18.37	17.79	17.52	0.86	0.83	0.85	2.03	b
145	323.901374	57.67494	19.29	17.44	16.81	16.53	0.31	0.27	0.35	1.61	b
147	323.909808	57.932454	17.28	15.52	14.96	14.66	0.30	0.32	0.22	2.42	c
149	323.91459	57.679216	17.83	15.89	15.24	14.85	0.18	0.10	0.32	1.20	a
150 <sup>b</sup>	323.923444	57.829681	20.52	18.77	18.23	17.79	0.41	0.58	0.37	1.10	b
151	323.926653	57.274163	17.31	16.07	15.71	15.50	0.18	0.20	0.21	1.15	b
152	323.927697	57.84018	18.94	16.83	16.01	15.60	0.07	0.16	0.17	1.08	a
153 <sup>b</sup>	323.92776	57.782978	20.78	18.41	17.92	17.41	0.26	1.34	1.37	3.31	a
154	323.938508	57.407235	20.18	17.69	16.71	16.28	0.24	0.39	0.44	0.83	a
155 <sup>b</sup>	323.93954	57.975013	20.44	18.71	18.12	17.76	0.82	0.59	0.58	1.13	c
158	323.948391	57.800469	16.94	15.22	14.58	14.24	0.32	0.24	0.31	2.68	b
159	323.948881	57.443986	16.10	14.60	14.14	13.84	0.14	0.15	0.19	1.01	a
160 <sup>b</sup>	323.964082	57.308463	21.49	18.69	17.86	17.39	0.94	0.41	0.43	2.02	c
161	323.981452	57.987654	18.47	16.97	16.54	16.25	0.20	0.24	0.31	1.63	a
162	323.987812	58.055186	19.77	17.98	17.26	16.94	0.30	0.33	0.44	1.98	a
164	323.99558	57.766371	18.06	16.46	15.90	15.63	0.13	0.17	0.25	1.17	a
165 <sup>b</sup>	324.009793	57.55542	20.24	18.32	17.35	17.01	0.64	0.60	0.55	1.08	b
167	324.013218	57.365742	17.98	15.96	15.25	14.88	0.19	0.19	0.19	1.77	b
169 <sup>b</sup>	324.020839	57.236011	20.74	19.03	18.27	17.96	0.81	0.68	1.10	0.85	a
170	324.023323	57.734711	16.50	15.05	14.58	14.33	0.42	0.44	0.42	1.83	b
171	324.027945	57.749176	19.12	17.42	16.82	16.54	0.17	0.10	0.13	1.09	b
172	324.036099	58.074033	17.59	16.02	15.49	15.22	0.06	0.12	0.09	1.08	a
173	324.050403	57.404812	19.89	18.16	17.35	16.93	0.58	0.52	0.42	1.71	c
175 <sup>c</sup>	324.06935	57.477867		16.76	15.12	13.88	0.17	0.17	0.23	1.73	a
177 <sup>b</sup>	324.073466	57.637216	20.43	18.57	17.95	17.72	0.52	0.20	0.32	1.04	c
178	324.07555	57.256661	18.64	16.59	15.74	15.39	0.25	0.18	0.16	1.04	c
179	324.080179	57.750692	18.71	16.85	16.11	15.80	0.29	0.12	0.11	1.02	c
180	324.085655	57.301582	14.20	13.20	12.97	12.81	0.09	0.09	0.06	0.96	c
181	324.095998	57.500881	18.81	16.92	16.16	15.81	0.33	0.28	0.26	1.90	b
183	324.099234	57.892217	17.29	15.87	15.39	15.19	0.23	0.22	0.26	1.90	b
184	324.114402	57.481949	21.66	18.52	17.24	16.56	0.50	0.41	0.39	1.70	b
185 <sup>b</sup>	324.128405	57.216288	19.94	18.19	17.52	17.24	0.34	0.36	0.38	1.32	b
187 <sup>b</sup>	324.140246	57.986823	20.70	18.88	18.19	17.88	0.58	0.54	0.82	1.12	a
188 <sup>b</sup>	324.14659	57.717027		19.55	18.39	18.22	1.61	1.08	0.98	0.95	c
189	324.149719	57.674449	18.77	17.22	16.61	16.36	0.33	0.33	0.27	1.80	b
190	324.154462	57.530351	21.98	18.85	17.80	17.20	0.58	0.46	0.47	1.79	b
191	324.157877	57.244062	16.22	14.93	14.44	14.22	0.41	0.38	0.38	3.60	b
194	324.174182	57.242164	18.50	17.05	16.46	16.35	0.13	0.47	0.46	2.14	a
195	324.202567	57.428411	16.13	14.92	14.50	14.34	0.26	0.26	0.25	1.02	b
196	324.204219	57.981013	18.86	16.68	15.98	15.53	0.31	0.27	0.32	1.74	b
197 <sup>b</sup>	324.206769	57.755108	19.78	18.11	17.57	17.31	0.45	0.49	0.49	2.55	b
198	324.220807	57.913238	16.39	14.99	14.37	14.10	0.11	0.11	0.15	1.07	a
199	324.224411	57.569493	18.42	16.99	16.62	16.41	0.43	0.41	0.37	4.48	b
200	324.229618	57.413448	16.79	15.40	14.94	14.75	0.11	0.08	0.10	1.01	b
201	324.230768	57.346378	19.13	17.16	16.54	16.20	0.31	0.60	0.42	1.13	a
202 <sup>b</sup>	324.232413	57.877623		18.48	17.66	17.07	1.30	1.31	1.83	8.64	a
203	324.234015	57.842234	18.39	16.95	16.36	16.14	0.69	0.59	0.61	4.78	b
204	324.237413	57.489649		16.84	14.58	13.06	0.41	0.47	0.60	3.69	a

Table 4 — *Continued*

ID	RA	DEC	I	J	H	K	$\Delta J$	$\Delta H$	$\Delta K$	$\langle S \rangle$	var type <sup>a</sup>
205 <sup>b</sup>	324.241394	57.225253		19.28	18.66	18.10	0.57	1.21	0.81	1.04	a
211	324.25944	57.428327		17.26	16.84	16.35	0.55	0.56	0.61	2.85	b
213	324.264693	57.924679	18.03	16.69	16.37	16.22	0.27	0.22	0.25	2.02	b
215	324.274313	57.425265	17.71	15.63	14.91	14.49	0.32	0.24	0.28	3.12	b
217	324.279074	57.646807	18.37	16.85	16.42	16.24	0.28	0.20	0.22	0.71	b
219	324.292339	57.880517	17.65	16.25	15.74	15.58	0.27	0.24	0.28	1.63	b
221 <sup>b</sup>	324.300192	57.60862	19.67	17.85	17.22	17.00	0.71	0.49	0.44	1.97	c
223	324.30335	57.767367	16.73	15.19	14.48	14.27	0.54	0.42	0.54	3.31	b
224 <sup>b</sup>	324.303574	57.867436	20.50	18.68	18.04	17.86	0.53	0.48	0.58	1.12	b
226 <sup>b</sup>	324.31021	57.981024	20.84	19.18	18.34	18.07	0.50	0.68	0.85	1.07	a
228	324.311431	57.649135	19.34	17.53	16.82	16.62	0.22	0.27	0.34	1.25	a
229	324.311723	57.563683	17.16	15.77	15.30	15.16	0.05	0.10	0.15	1.07	a
230 <sup>b</sup>	324.312393	57.31857	20.41	18.57	18.02	17.74	0.54	0.58	0.49	1.34	b
233	324.32337	57.413722	16.27	14.99	14.49	14.33	0.09	0.06	0.23	1.01	a
234	324.329549	57.559674	16.54	14.93	14.41	14.15	0.29	0.28	0.28	2.80	b
235	324.331403	57.886321	19.03	16.81	16.15	15.74	0.38	0.34	0.40	1.23	b
236	324.332425	58.046772	15.64	14.40	14.03	13.75	0.10	0.07	0.11	0.71	b
237 <sup>b</sup>	324.332613	58.027099	20.23	18.46	17.88	17.55	0.74	0.76	1.02	2.50	a
238 <sup>b</sup>	324.334189	57.852993	20.70	18.76	17.90	17.57	0.49	0.46	0.55	1.15	b
239 <sup>b</sup>	324.335617	57.83023	21.70	19.42	18.52	18.11	0.49	0.64	0.69	1.42	b
240 <sup>b</sup>	324.335815	57.224303	20.86	19.23	18.61	18.13	1.51	1.00	0.79	1.41	c
241 <sup>b</sup>	324.33879	57.853015	20.23	18.67	18.13	17.80	0.50	0.60	0.78	1.04	a
244 <sup>b</sup>	324.365299	57.70495	21.09	19.02	17.96	17.04	0.56	0.68	0.79	2.07	a
245 <sup>b</sup>	324.365598	57.695278		19.20	18.62	17.99	1.39	1.93	1.60	1.68	b
246	324.365724	57.418122	19.00	17.32	16.72	16.47	0.71	0.67	0.57	3.95	b
248 <sup>b</sup>	324.368122	57.988184	20.20	18.56	17.84	17.55	0.36	0.47	0.37	1.19	b
249 <sup>b</sup>	324.36935	57.700139		19.27	18.05	17.14	1.03	0.47	0.61	1.50	c
253	324.383148	57.532638	22.70	19.22	18.39	17.54	0.68	0.33	0.52	1.14	c
254	324.386412	57.459189	17.81	16.49	16.00	15.74	0.34	0.34	0.40	3.05	b
255	324.387789	57.475863	18.80	17.10	16.37	16.10	0.10	0.20	0.24	1.02	a
258	324.398652	58.026245	18.75	17.07	16.46	16.13	0.46	0.33	0.36	3.44	b
259 <sup>b</sup>	324.40393	57.309533	19.42	17.84	17.28	17.03	0.30	0.50	0.32	1.19	b
261 <sup>b</sup>	324.405461	57.816849	19.86	18.15	17.66	17.40	0.67	0.75	0.41	1.85	c
263 <sup>b</sup>	324.415486	57.522071	19.83	18.13	17.51	17.21	0.52	0.68	0.54	2.83	b
264	324.415765	57.364344	18.55	17.07	16.59	16.38	0.22	0.28	0.26	1.56	b
265	324.418829	57.396573	19.45	17.70	16.99	16.72	0.39	0.37	0.32	0.99	b
266 <sup>b</sup>	324.420296	57.38383		19.26	18.29	17.54	0.94	0.54	0.30	1.14	c
267	324.421722	57.623431	16.77	15.57	15.14	14.94	0.87	0.72	0.72	5.92	b
268	324.426649	57.213716	15.25	13.92	13.50	13.25	0.09	0.08	0.10	0.95	b
269	324.428263	57.48672	16.26	14.89	14.38	14.15	0.20	0.19	0.20	1.88	b
274	324.454563	57.491008	18.17	16.66	16.16	15.90	0.18	0.18	0.16	1.55	b
277 <sup>b</sup>	324.461205	57.826255	20.35	18.35	17.67	17.38	0.52	0.43	0.55	2.08	b
279 <sup>c</sup>	324.466475	57.577636	19.61	18.04	17.48	17.27	0.64	0.43	0.49	1.39	b
281	324.46901	57.432259		18.67	17.26	16.12	0.44	0.55	0.73	2.13	a
282	324.470107	57.430347	19.04	17.55	16.99	16.75	0.34	0.48	0.34	1.86	b
284	324.482278	57.733467	18.29	16.77	16.22	16.01	0.23	0.28	0.34	0.80	a
285	324.482373	57.950863	19.46	17.79	17.27	16.98	0.41	0.50	0.40	2.76	b
286	324.483023	57.952424	18.53	17.22	16.83	16.58	0.53	0.52	0.54	2.32	b
287	324.488459	57.984369	17.27	15.86	15.41	15.16	0.24	0.21	0.23	2.70	b
290 <sup>b</sup>	324.49291	57.970182	19.33	17.65	17.06	16.84	0.17	0.30	0.14	1.01	b
296	324.525974	57.547971	17.45	16.09	15.61	15.41	0.21	0.19	0.19	1.39	b
297	324.530946	57.721721	18.22	16.76	16.27	16.03	0.33	0.30	0.32	3.04	b
298 <sup>b</sup>	324.534461	57.42341	19.52	17.87	17.23	17.02	0.75	0.26	0.32	1.99	c
299	324.54104	58.002596	19.65	17.53	16.74	16.33	0.24	0.26	0.23	1.67	b
300	324.546493	57.819141	19.12	17.33	16.76	16.45	0.31	0.27	0.24	0.87	b
301	324.549082	57.513066	17.15	15.91	15.47	15.26	0.23	0.29	0.16	1.24	c
302	324.549274	57.353128	14.35	13.28	12.84	12.68	0.67	0.57	0.58	5.29	b
303	324.549659	57.455694	17.23	16.05	15.64	15.45	0.26	0.27	0.23	0.99	b
306	324.564617	57.695576	17.00	15.68	15.23	15.04	0.39	0.35	0.30	2.37	c
308 <sup>b</sup>	324.570825	57.257867	20.19	18.62	17.89	17.71	0.49	0.75	0.63	2.60	b
309	324.576107	57.627173	15.87	14.51	13.94	13.75	0.09	0.10	0.11	0.80	b
310	324.578854	57.891238	16.15	14.82	14.41	14.19	0.22	0.20	0.20	2.29	b
311	324.579683	57.565231	14.32	13.44	13.23	13.11	0.08	0.11	0.11	0.94	a
312 <sup>b</sup>	324.580803	57.398289		18.50	17.38	16.47	0.35	0.56	0.44	1.46	b
313	324.583337	57.817748	18.06	16.04	15.20	14.88	0.12	0.10	0.10	0.97	b
314	324.587159	58.001805	18.74	17.01	16.41	16.12	0.15	0.20	0.19	1.18	b
315 <sup>b</sup>	324.588839	57.604719	20.03	18.32	17.53	17.29	0.75	0.71	0.82	2.41	b
318	324.602574	57.460107	17.09	15.80	15.43	15.21	0.28	0.26	0.27	3.76	b
319	324.60358	57.976906	17.92	16.04	15.29	14.97	0.19	0.13	0.13	1.19	c
321	324.611961	57.629291	18.11	16.48	15.95	15.70	0.15	0.16	0.15	1.45	b
322 <sup>b</sup>	324.612926	57.681887	19.50	17.89	17.40	17.17	0.47	0.51	0.55	2.59	b
323	324.61299	57.312357	17.54	16.22	15.78	15.58	0.32	0.39	0.42	1.85	b
325 <sup>b</sup>	324.616936	57.583752	19.94	18.82	18.18	17.87	0.89	0.62	0.85	1.55	b

Table 4 — *Continued*

ID	RA	DEC	<i>I</i>	<i>J</i>	<i>H</i>	<i>K</i>	$\Delta J$	$\Delta H$	$\Delta K$	$\langle S \rangle$	var type <sup>a</sup>
326	324.6177	57.841105	18.91	16.91	16.07	15.74	0.25	0.33	0.50	0.89	a
328 <sup>b</sup>	324.619441	57.499178		19.25	18.44	18.09	1.02	0.98	0.86	1.34	b
334	324.650439	57.839356	17.51	16.17	15.78	15.60	0.26	0.26	0.28	2.64	b
335 <sup>c</sup>	324.651351	57.700962	19.00	17.48	17.03	16.76	0.30	0.29	0.27	1.55	b
336	324.657752	58.072764	19.14	17.42	16.77	16.49	0.46	0.38	0.48	3.92	b
337	324.659975	57.770895	17.95	16.51	16.02	15.85	0.17	0.17	0.19	1.46	b
339 <sup>b</sup>	324.673815	57.501893	19.72	18.34	17.83	17.41	0.54	0.77	0.58	3.07	b
343 <sup>b</sup>	324.685325	57.471052		18.89	17.92	17.41	1.06	0.68	0.59	2.10	c
344	324.689726	57.633382	15.26	13.87	13.21	13.01	0.12	0.09	0.10	0.75	b
345 <sup>b</sup>	324.703238	58.002556		19.35	17.76	17.43	0.88	1.17	1.47	1.10	a
346	324.703928	57.350577		18.42	17.25	16.40	1.41	0.72	0.51	2.98	c
349	324.71218	57.475678	16.24	14.29	13.51	13.16	0.23	0.18	0.14	1.41	c
351	324.717743	57.349315	22.12	18.82	17.55	16.64	0.54	0.43	0.68	2.28	b
352	324.72229	57.869437		17.14	16.75	16.52	0.38	0.51	0.79	1.86	a
353	324.72427	58.073583	16.68	15.33	14.81	14.66	0.21	0.08	0.15	1.07	c
356	324.729196	58.047909	19.50	17.30	16.34	16.00	0.26	0.25	0.25	2.13	b
357	324.732201	57.523745	16.49	15.41	14.99	14.86	0.31	0.29	0.16	1.64	c
358 <sup>b</sup>	324.735329	57.922575	20.12	18.44	17.75	17.52	0.46	0.44	0.67	1.43	a
359	324.739937	57.719962		17.50	16.73	16.35	0.64	0.38	0.48	1.15	c

<sup>a</sup> a = variability is > 30% larger in magnitudes at *K* than at *J*; b = variability is within 30% of the same in magnitudes at *J* and *K*; c = variability is > 30% larger at *J* than at *K*. The relative sizes of the variations in *J* and *K* provide hints of the type of variations: category “a” is likely to vary through instabilities at the inner edge of the circumstellar disk resulting in different exposure of the disk dust; category “c” can arise either through extinction or accretion hot spots; in general the ratio  $\Delta J/\Delta K$  is  $< 2$  for extinction variations and  $> 2$  for hot spot ones.

<sup>b</sup> These sources are sufficiently faint that the indication of variability might be influenced by fainter nearby sources below the detection limit, so the results for them are less reliable than for the brighter sources. In addition, the errors on their measurements are larger than the nominal 2% for bright sources.

<sup>c</sup> Listed as a possible cluster member by Errmann et al. (2013). For Sources 175 and 279, the lack of *I* magnitudes results in their not being selected in our CMD approach, so we do not have an independent measure of whether they are cluster members. Source 335 falls far from the zone for Tr 37 members on the *K*, *I* – *K* CMD, potentially calling its membership into question.

**Table 5**  
Summary of Variability Observed in Bright Members of Tr 37

ID	Sp. Type	RA	DEC	<i>RI</i> var.	<i>JHK</i> var.	<i>W1W2</i> var.	<i>W1 - W2<sup>f</sup></i>	accretion <sup>b</sup>	membership <sup>c</sup>
71-1309		21 34 09.74	+57 29 55.0		N	W1 >13	-		PN
74-48	-	21 34 47.30	+57 31 14.8		N/A	N	0.34		P
81-541	K5.5	21 35 17.45	+57 48 22.3		V	N	0.49	0.19	P
64-156	-	21 35 18.04	+57 09 44.1		N/A	conf.	-0.06		P
73-472	K5	21 35 18.61	+57 34 09.2		N/A, V(2M)	S	0.29		Y
73-311	M1.5	21 35 24.51	+57 33 01.1		V	S	0.51		P
73-71	K6	21 35 30.21	+57 31 16.4		N/A	conf.	0.36		Y
72-875	M0.5	21 35 49.75	+57 24 04.1	BP, SB	N/A	S	0.51	0.11	PN
61-608	-	21 35 50.70	+57 03 57.0		N/A	N <sup>k</sup>	-0.06		Y <sup>l</sup>
61-893	-	21 36 00.90	+57 07 12.9		V	N	-0.08		P
73-537	G1.5	21 36 07.23	+57 34 32.4		N/A	N <sup>j</sup>	-0.14		Y
84-23	-	21 36 12.81	+57 53 00.4		N/A	conf.	-		Y
61-413	-	21 36 26.15	+57 01 29.3		N/A	W1 > 13	-0.21 <sup>h</sup>		PN
14-306	K6.5	21 36 26.76	+57 32 37.4		N/A	conf.	0.12		P
14-141	K6	21 36 49.41	+57 31 22.0	BP, F(S-A)	Sat., V(2M)	conf., V <sup>i</sup>	0.41 <sup>i</sup>	< 2.3	Y
14-1229	K6	21 36 55.79	+57 36 53.3		N	W1 >13	-		P
11-2146	K6	21 36 57.67	+57 27 33.1	BP, F(S-A)	Sat., V(2M)	S/F <sup>j</sup> , V <sup>i</sup>	0.60	0.99	Y
11-1209	K6	21 36 58.55	+57 23 26.1	F(S-A)	N/A	S/F <sup>k</sup>	0.28	0.56	Y <sup>l</sup>
11-1659	K5	21 37 00.88	+57 25 22.4		V	N	-0.08	0	Y
11-1499	M1.5	21 37 01.40	+57 24 45.8		N/A	conf.	-	0	P
11-2322	M1	21 37 01.91	+57 28 22.2	BP, F(S-A)	N/A	N <sup>j</sup> , V <sup>i</sup>	0.38	1.6	Y
11-1871	M2	21 37 02.54	+57 26 14.4		N/A	N <sup>k</sup>	0.07		P
14-222	K7	21 37 06.07	+57 32 01.8	F(S-A)	Sat., V(2M)	N	0.01	< 0.04	P
14-287	M0	21 37 06.49	+57 32 31.6	BP	N/A	S/F <sup>k</sup> , V <sup>i</sup>	0.51	0.21, 0.46	Y
11-2037	K4.5	21 37 07.07	+57 27 01.1	F(S-A)	V	N	0.43	< 9	Y
11-1067	0.5	21 37 08.43	+57 22 48.4		N	W1 >13	-0.01 <sup>d</sup>	0	P <sup>l</sup>
14-11	M1.5	21 37 10.31	+57 30 18.9		N/A	N <sup>k</sup> , N <sup>i</sup>	0	Y	
14-125	K5	21 37 10.54	+57 31 12.6	F(S-A)	N/A	N <sup>k</sup> , V <sup>i</sup>	0.42	0.34	Y
14-1827 <sup>a</sup>	G	21 37 11.26	+57 39 17.3	SB, F(S-A)	N/A	N	-0.02		PY <sup>l</sup>
11-1513	K7.5	21 37 11.83	+57 24 48.6		V	N	0.06	0	P
11-2131	K6.5	21 37 12.19	+57 27 26.6	BP, SB	V, V(2M)	S:	0.45	0.25	P
11-2487	K7	21 37 14.98	+57 29 12.3		N	N	0.04		P
11-2031	K2	21 37 15.95	+57 26 59.5	BP, F(S-A)	Sat., V(2M)	F	0.48	< 1	Y
14-103	K7	21 37 19.76	+57 31 04.3		N	conf.	-	0	P
14-197	K5.5	21 37 23.68	+57 31 53.8		N/A	N	0.08	< 0.14	P:
14-160	K5	21 37 27.33	+57 31 29.7	BP, F(S-A)	N/A	S/F	0.63		Y
11-581	G	21 37 28.34	+57 20 33.1	F(S-A)	N/A	conf.	-0.09 <sup>d</sup>	0	PN
14-1017	M0	21 37 28.95	+57 36 04.7	F(S-A)	V	S/F	0.60	< 0.5	P
14-335	K6.5	21 37 29.09	+57 32 52.8	SB, F(S-A)	Sat., N(2M)	S <sup>j</sup>	0.59	< 0.14	P
11-1180 <sup>a</sup>	G-K	21 37 30.63	+57 23 17.9		N/A	W1 >13	-0.19		PN
11-1864	G-K	21 37 34.28	+57 26 15.8		N/A	N <sup>j</sup>	0.00		PN
83-343	M0.5	21 37 36.96	+57 55 14.9	BP:	N/A	N <sup>j</sup>	0.25	< 0.1	Y
14-183	K7.0(K5)	21 37 38.53	+57 31 41.7	SB	N/A	conf.	0.24	0.16	P:
14-995	-	21 37 39.87	+57 36 02.9		N/A	W1 >13	-0.02		PN
11-1721 <sup>a</sup>	K5	21 37 41.16	+57 25 41.0		N	F:	-0.10		PN
14-2148	M1.5	21 37 41.84	+57 40 40.0		N/A	N <sup>k</sup>	-0.01	0	Y
	F9	21 37 42.75	+57 33 25.0		Sat., V(2M)	S	0.67		P
11-1384	K6.5	21 37 44.86	+57 24 13.5		N/A	N <sup>j</sup>	0.04	0	P
11-383	K5	21 37 45.16	+57 19 42.7	F(S-A)	V	S	0.72		P
11-2318 <sup>a</sup>	M0	21 37 45.22	+57 28 18.0	F(S-A)	N/A	N	-0.12		Y
		21 37 48.93	+57 23 20.9		V	N	0.34		P
13-924	K5	21 37 50.26	+57 33 41.3		V	N	0.05	0	Y
12-1984	K6	21 37 50.22	+57 25 48.7	BP	V	N	0.07	0/0.6	P
12-2519	K5.5	21 37 51.07	+57 27 50.2		N/A	N	0.37	0.07	Y
12-1968	K6	21 37 54.87	+57 26 42.4		N/A	conf.	-	0.34	Y
12-1422	M0	21 37 57.63	+57 24 20.2	BP, F(S-A)	N/A	conf.	-	< 0.24	P
12-1091	G2.5	21 37 57.68	+57 22 48.2	BP	V, V(2M)	S	0.45	< 0.4	Y
13-269	K6.5	21 37 58.12	+57 31 19.9		V, V(2M)	F::	0.08	0/< 0.1	P
12-583	M0	21 37 58.36	+57 20 36.0	F(S-A)	N/A	conf.	0.16	0	P
12-94	K4	21 37 58.52	+57 18 05.5		N/A	conf.	-		P
13-1143	-	21 37 58.52	+57 35 47.9		N/A	conf.	-		P
13-1238	M1	21 37 59.28	+57 36 16.7	BP, F(S-A)	N	F/S::	0.55	0.6	P
12-2373	M1	21 38 00.58	+57 28 25.3		N/A	conf.	0.53	0	Y
82-272	G9	21 38 03.50	+57 41 34.9	SB	Sat., V(2M)	N	0.50	< 0.9	Y
12-1081	M0.5	21 38 05.99	+57 22 44.4	SB, F(S-A)	V, V(2M)	N	0.01	0	P
13-1161	M0	21 38 07.74	+57 35 53.8		N	N	-0.08	0	Y
12-1613	M1	21 38 08.52	+57 25 12.4		N/A	conf.	0.08	0	P
13-1426	M0	21 38 08.57	+57 37 08.2	SB, F(S-A)	N/A	S	0.58	0.6	P
	-	21 38 09.24	+57 20 19.8	SB	N/A	N	0.42		Y
13-669	K1	21 38 09.30	+57 33 26.7		N/A	N	0.48	0.58	Y
	-	21 38 09.79	+57 29 42.8	BP	N	N	0.40		Y

Table 5 — *Continued*

ID	Sp. Type	RA	DEC	<i>RI</i> var.	<i>JHK</i> var.	<i>W1W2</i> var.	$W1 - W2^f$	accretion <sup>b</sup>	member- ship <sup>c</sup>
13-838	–	21 38 11.20	+57 34 18.1		N	N	-0.04		PN
13-350	M1	21 38 13.82	+57 31 42.5	SB	N/A	N <sup>j</sup>	0.18	0	Y
12-1017	K5.5	21 38 15.09	+57 21 55.4		N/A	N <sup>j</sup>	0.05		Y
54-1781	M1	21 38 16.12	+57 19 35.7		V	S/F	0.37	0.3	Y
13-1877	K7	21 38 17.03	+57 39 26.5	BP, SB	Sat., V(2M)	N	0.49	1.6	P
13-277	G1	21 38 17.36	+57 31 22.5		Sat., N(2M)	S	0.64	14	P:
13-2236	K6.5	21 38 17.49	+57 41 01.9		N/A	conf.	–		Y
12-1009	K5.5	21 38 17.50	+57 22 30.8		N/A	conf.	–	0.07	Y
94-1119	–	21 38 18.62	+58 03 28.3		N	N	-0.04		P
13-819	K5.5	21 38 25.96	+57 34 09.3	BP	V	N	0.09	< 0.14	P
94-1050	–	21 38 26.68	+58 02 37.7		N	conf.	–		Y
12-1955	K6.5	21 38 26.96	+57 26 39.0	BP:	N/A	N	0.01	0	Y
13-236	K2	21 38 27.46	+57 31 08.6		Sat., V(2M)	N	0.46	0.51	Y
12-2113	K6	21 38 27.47	+57 27 21.3	F(S-A)	Sat., N(2M)	S	0.57		PN
13-157	K5.5	21 38 28.04	+57 30 46.4	SB:	Sat., N/A (2M)	conf.	–	4.2	Y
12-232	M0	21 38 28.34	+57 31 07.2		N/A	conf.	–	0	P
	M0	21 38 32.16	+57 26 35.9		N/A	F	0.44 <sup>e</sup>	0.4	P
13-52	K7	21 38 32.55	+57 30 16.1	BP	N/A	conf.	0.16		Y
12-1825	–	21 38 33.85	+57 26 05.9	SB	N	N	0.03		Y
91-155	M2.5	21 38 34.70	+57 41 27.4		N/A	conf.	–		Y
13-566	K5.5	21 38 34.81	+57 32 50.0		N	N	-0.01	0	P
13-1891	M0	21 38 40.01	+57 39 30.3		N/A	conf.	–		Y
13-1709	K5.5	21 38 40.38	+57 38 37.4	SB	V	N	0.01	0	Y
12-44 <sup>a</sup>	K4	21 38 44.50	+57 18 09.5	BP	N/A	S/F	0.36		Y
54-1613	K5	21 38 43.32	+57 18 35.9		V	N	-0.04	0	Y
	M2	21 38 43.50	+57 27 27.0		V	F	0.56	0	P
54-1547	K5.5	21 38 44.46	+57 18 09.1	BP, SB	N/A	???	0.36	0.21, 0.18	Y
12-2363	M0.5	21 38 45.44	+57 28 23.0		N/A	N <sup>j</sup>	-0.07	0	P:
12-595	K7	21 38 46.29	+57 20 38.8	SB	N/A	conf.	-0.05 <sup>d</sup>	0	P
12-1423	K7	21 38 47.07	+57 24 20.7		N/A	N <sup>k</sup>	0.04	0	Y
12-1010	M2	21 38 50.29	+57 22 28.3		N/A	conf.	0.45	0.04	Y
12-2098	M2.5	21 38 52.53	+57 27 18.4		N/A	conf.	–	0	P
21-851	–	21 38 55.04	+57 20 42.3		N/A	W1>13	-0.02 <sup>d</sup>		Y
13-1087	K4	21 38 55.42	+57 35 29.9		N/A	conf.	–		Y
91-506	K6.5	21 38 58.07	+57 43 34.3	BP	N/A	conf.	0.34	0.09	Y

<sup>a</sup> Only listed in Sicilia-Aguilar et al. (2004).<sup>b</sup> From Sicilia-Aguilar et al. (2010).<sup>c</sup> From Sicilia-Aguilar et al. (2006b): Y & Y indicated as Y; Y & P indicated as Y; P & P indicated as P; Y indicated as P; P indicated as P; Y & PN indicated as P; Y & N indicated as PN; PN indicated as PN.<sup>d</sup> Indicated error 0.04 to 0.06<sup>e</sup> Indicated error 0.06 to 0.08<sup>f</sup> From ALLWISE, errors of 0.03 to 0.04 unless otherwise indicated<sup>g</sup> Very bright star (5th mag) within 90"; detection possibly contaminated by scattered light halo<sup>h</sup> Two very bright stars (6th mag) within 2"; detection possibly contaminated by diffraction spike<sup>i</sup> From Morales-Calderón et al. (2009).<sup>j</sup> Very close fainter object that is integrated into the WISE PSF with little effect, but undermines the PSF fitting with the UKIRT data given its ~ six times higher resolution.<sup>k</sup> A nearby source interferes with the UKIRT PSF fitting but is outside the region where the WISE deblending is not valid.<sup>l</sup> Gaia parallax suggests this object is foreground to the cluster.

**Table 6**  
Summary of Variability Observed in Members of Tr 37 from Sicilia-Aguilar et al. (2013)

Source	$RA_{opt}$	$DEC_{opt}$	$RA_{IR}$	$DEC_{IR}$	$J$	$H$	$K$	$J_{amp}$	$H_{amp}$	$K_{amp}$	var.
S13-006	324.093260	57.528118	324.093262	57.528101	14.644	13.867	13.409	0.063	0.065	0.049	N
S13-013	324.172322	57.367809	324.172327	57.367830	15.200	14.511	14.165	0.138	0.148	0.140	V
S13-016	324.221700	57.347809	324.221745	57.347835	15.419	14.719	14.416	0.040	0.036	0.039	N
S13-020	324.246250	57.651722	324.246244	57.651560	13.459	12.649	12.180	0.163	0.240	0.247	V
S13-021	324.247917	57.526389	324.247785	57.526337	14.500	13.434	12.625	0.213	0.244	0.333	V
S13-022	324.255320	57.571840	324.255526	57.571777	14.657	13.863	13.486	0.113	0.111	0.121	V
S13-025	324.263400	57.455160	324.263386	57.455113	14.462	13.683	13.395	0.097	0.091	0.108	V
S13-027	324.282125	57.536389	324.282135	57.536412	14.622	13.853	13.459	0.056	0.066	0.085	N
S13-033	324.295342	57.646355	324.295371	57.646366	15.767	15.132	14.742	0.056	0.047	0.092	N
S13-035	324.302140	57.682050	324.302410	57.681969	16.006	15.306	14.966	0.033	0.033	0.055	N
S13-036	324.318333	57.444611	324.318156	57.444543	13.904	12.936	12.376	0.496	0.450	0.404	V
S13-037	324.336000	57.350159	324.336000	57.350125	14.712	13.969	13.647	0.062	0.065	0.084	N
S13-041	324.358960	57.391823	324.358939	57.391881	15.853	15.221	14.780	0.043	0.051	0.062	N
S13-048	324.392132	57.575333	324.392136	57.575332	14.786	13.855	13.243	0.670	0.505	0.347	V
S13-049	324.394583	57.282667	324.394358	57.282700	14.748	13.894	13.331	0.249	0.217	0.236	V
S13-051	324.412083	57.493694	324.411844	57.493595	13.282	12.428	11.857	0.342	0.226	0.301	V
S13-052	324.417572	57.317699	324.417636	57.317629	15.311	14.719	14.262	0.025	0.028	0.034	N
S13-053	324.418663	57.575901	324.418669	57.575880	14.931	14.148	13.718	0.073	0.055	0.063	N
S13-056	324.432873	57.581165	324.432851	57.581181	15.310	14.606	14.114	0.164	0.155	0.120	V
S13-060	324.437917	57.328472	324.438118	57.328395	13.764	12.938	12.321	0.259	0.327	0.435	V
S13-063	324.451012	57.388725	324.451059	57.388709	14.690	13.986	13.630	0.050	0.055	0.034	N
S13-064	324.453895	57.389156	324.453945	57.389145	15.108	14.024	13.285	1.108	0.705	0.413	V
S13-069	324.463333	57.410056	324.463395	57.410042	15.430	14.713	14.176	0.193	0.238	0.241	V
S13-070	324.486573	57.580048	324.486574	57.580002	15.566	14.820	14.455	0.056	0.086	0.053	N
S13-073	324.538429	57.343922	324.538464	57.343900	15.730	15.100	14.710	0.097	0.098	0.104	N
S13-077	324.550000	57.416889	324.550068	57.416890	14.482	13.684	13.300	0.469	0.435	0.444	V
S13-079	324.567204	57.326611	324.567262	57.326586	13.963	13.191	12.817	0.179	0.161	0.184	V
S13-081	324.580884	57.367752	324.580961	57.367837	15.765	15.228	14.837	0.033	0.034	0.030	N <sup>a</sup>
S13-084	324.599801	57.460049	324.599777	57.460071	14.834	14.043	13.635	0.128	0.122	0.102	V
S13-088	324.616795	57.793453	324.616835	57.793438	15.401	14.671	14.245	0.193	0.173	0.097	V
S13-089	324.622371	57.624046	324.622351	57.624034	15.470	14.784	14.411	0.038	0.051	0.049	N
S13-090	324.626250	57.548750	324.626305	57.548660	14.936	14.129	13.596	0.238	0.194	0.140	V
S13-091	324.626667	57.438389	324.626473	57.438407	14.497	13.704	13.331	0.098	0.093	0.222	V

<sup>a</sup> Probable foreground star from Gaia parallax